

Stability of Neutron-Dark Matter Mixed Stars and Hybrid Stars

Xiao-Ding Zhou,^{1,*} Tian-Shun Chen,^{1,†} Si-Man Wu,^{1,‡} and Kilar Zhang^{1,2,3,§}

¹*Department of Physics and Institute for Quantum Science and Technology, Shanghai University, Shanghai 200444, China*

²*Shanghai Key Lab for Astrophysics, Shanghai 200234, China*

³*Shanghai Key Laboratory of High Temperature Superconductors, Shanghai 200444, China*

Concerning the stability of two-fluid star models, we prove the rigorous equivalence of two independent determining methods for mixed stars, after a brief review of the hybrid star case. Our derivations apply to general multi-fluid cases, and here we take dark matter admixed neutron star models for example, demonstrating a stability boundary distinct from the single-fluid case. Stable configurations form a surface in the three-dimensional parameter space of (either) central pressure, mass, and radius, which yields a group containing stable mixed stars. This group includes “twin stars” with identical masses and radii but different interior structures. These results can help interpret compact star observations and constrain dark matter properties through astrophysics.

I. INTRODUCTION

Evaluating the stability of compact stars is an important issue in astrophysics, especially in the multi-messenger era marked by the gravitational wave observation of neutron stars (NS) [1]. For single fluid models, the stability criteria has two equivalent expressions, one from judging the sign of fundamental radial oscillation frequencies [2], the other from finding the extrema in mass-radius (M - R) curves (known as BTM criteria [3] by Bardeen, Thorne, and Meltzer). The first is time consuming but also gives higher oscillation modes, and works for multi-fluid case. The second method is intuitive and convenient, but its extension to multi-fluid case is not guaranteed.

There are mainly two scenarios for multi-fluid star structures, hybrid stars [4–7] when the interactions among different fluids are strong, and mixed stars [8–17] when the interactions except gravitational ones are negligible. Hybrid star case is relatively simple, and its stability rule is found in [7]. As a byproduct in another work [17], other collaborators and one of the current authors have conjectured necessary conditions from BTM criteria for mixed stars, which needs further modifications. In fact, for mixed star case, there are two known independent approaches for determining the stability. One is through calculating the radial oscillation frequencies [2, 18] as mentioned before, and the other is from finding the parallel critical curves in certain parameter space [8]. Their equivalence is argued in [8] and checked for specific EoS in [19]. In this paper, we give a rigorous proof of this equivalence (and for multi-fluid case in the companion paper [20]), and further explore its application to dark matter (DM) - nuclear matter (NM) mixed stars.

NS, with extremely high compactness, serve as natural laboratories for testing theoretical physics. As relativistic

objects, they should be described within the framework of General Relativity. Their macroscopic properties (such as mass and radius) are determined by the Tolman-Oppenheimer-Volkoff (TOV) equations [21, 22] describing gravitational equilibrium, and the equation of state (EoS) governing microscopic nuclear interactions [23]. In our discussion, these objects are treated at zero temperature as commonly applied. Consequently, the pressure is treated as depending solely on the energy density.

The evidences for the existence of DM are various, including galactic rotation curves, large-scale structure formation, and gravitational lensing [24]. Precise cosmological observations and measurements further indicate that DM constitutes approximately 25% of the total energy budget the universe [25].

At particle physics level, one of the DM candidates is the Weakly Interacting Massive Particle (WIMP), such as the neutralino in supersymmetric theories, whose thermal production mechanism can naturally explain the DM abundance [26, 27]. Beyond the traditional WIMP paradigm, DM may possess other properties. For example, models of Asymmetric DM, where the DM particle is not self-conjugate [28, 29], provide another promising theoretical framework.

Additionally, DM could be bosonic particles with self-interactions, which would affect its dynamic evolution within NS [27]. This so called Self-interacting Dark Matter (SIDM) extends the standard conventional cold DM model by incorporating self-interactions, which can effectively mitigates small-scale structure issues [30, 31]. A key constraint on this model requires the ratio of its self-scattering cross-section to the mass to lie within a small window [30, 32, 33]. SIDM provides a theoretical possibility to form compact star structures [34].

DM detection strategies are primarily divided into direct and indirect detections. Direct detection experiments (e.g., DAMA, CoGeNT, CDMS, XENON [35–38]) aim to receive signals from the scatterings of DM particles on atomic nuclei within detectors [39]. Indirect detection, on the other hand, is achieved by studying the effects of DM on astrophysical objects. For instance, the extremely strong gravitational field and high den-

* 18038288465@shu.edu.cn

† cts2003912@shu.edu.cn

‡ 2045152271@qq.com

§ kilar@shu.edu.cn; Corresponding Author

sity of NM in NS may make them possible DM trappers. Subsequent physical changes (such as heating, accumulating or collapse) in NS can then be used to constrain the properties of DM [27]. To be specific, the mechanisms by which DM may become captured into NS have been explored by many researches [40–46]. Should the captured DM be self-annihilating, its subsequent annihilation can significantly heat the star interior, leading to observable increases in surface temperature or luminosity [41–43]. In contrast, non-annihilating DM would gradually accumulate within the star, potentially giving rise to stable mixed configurations [47], or alternatively, collapsing into black holes once the DM inside the NS reach their self-gravitating limit [27]. Beyond capture, an alternative proposal is that the collapse leading to NS formation could be triggered within a pre-existing DM halo [48–50], i.e. the incorporation of DM and NM may occur during the formation of compact objects.

There has been extensive research on the influence of DM on the properties of compact stars, such as [39, 51–53]. It is necessary to discuss the conditions for the stable existence of mixed stars composed of these components; relevant studies include, for example, [17, 19, 54–58]. Our study primarily focuses on mixed stars consisting of NM and SIDM or fermionic DM, and we systematically investigate their stability and macroscopic properties through different methods.

This paper is organized as follows. In Section II, we establish the theoretical framework for star modeling, detailing the geometric configurations, equilibrium equations in both single and multi-fluid formalism, and the EoS for both DM and NM components. Section III presents the comprehensive stability analysis methodology that we adopt, including the dynamic radial pulsation approach following [2, 19], and the critical point/curve method [3, 8] for static stability determination, and further rigorously demonstrating the equivalence between these two. Section IV shows our numerical findings, including stability boundary calculations for specific EoS combinations and analysis of macroscopic properties. Finally, Section V summarizes our key results and discusses the implications for constraining DM properties through astrophysical observations of compact stars. We put the detailed proof for equivalence between the two stability determining methods in appendix A.

II. STAR MODEL SETUP

To model the coexistence of DM and NM in compact astrophysical objects and their corresponding structure, we begin with a basic description of their possible internal composition, followed by the TOV equations for spherical equilibrium structure within the framework of General Relativity. The formulation is completed by specifying the EoS that relates pressure to energy density.

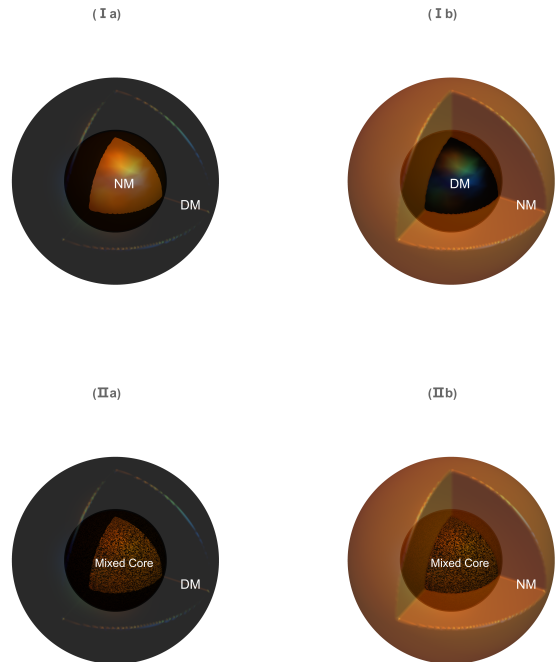


FIG. 1: Schematic diagram: two different possible structures: hybrid stars (I) and mixed stars (II).

A. Possible Mixing Models

From the perspective of geometric configuration, two-fluid star models can be preliminarily classified into two categories. Hybrid star: a NM (DM) core enveloped by a DM (NM) crust; mixed star: a mixed core enveloped by a single-component shell [17, 54]¹, as shown in Fig.1.

The formation mechanisms of the layered and mixed-core configurations are fundamentally different in the perspective of microscopic interactions. The emergence of a layered structure requires the existence of non-gravitational interactions [50] between DM and NM, such that the total energy of the two-component system in a phase-separated state is lower than that of the mixed state, whereas a mixed core arises when only gravitational interactions are present, lacking the driving force for a sharp interface.

This structural difference profoundly influences their macroscopic manifestations. In M - R relations, layered (Hybrid) models depend on a single parameter variation, with a clear evolutionary path of a one-dimensional curve. In contrast, mixed-core models exhibit more complex parameter dependence corresponding to the central parameters of both DM and NM, causing their M - R rela-

¹ In these two references, “Hybrid” includes both hybrid and mixed cases in this paper.

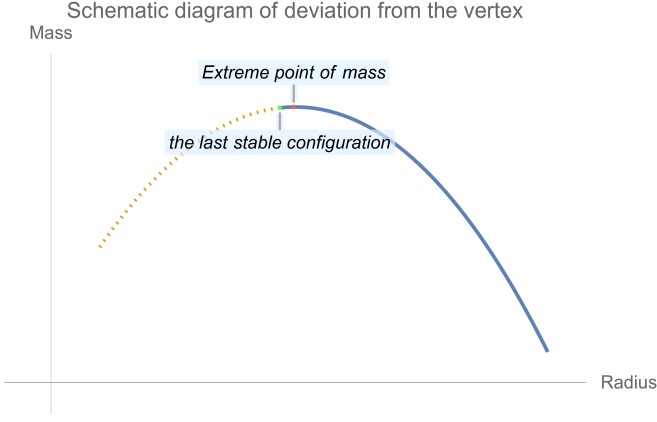


FIG. 2: Schematic diagram: the stability turning point of the hybrid star deviates from the mass vertex.

tion to topologically form a two-dimensional continuous surface.

Regarding stability, both types can have their stable regions rigorously determined via radial perturbation analysis. However, as the schematic diagram Fig.2 shows, unlike pure NS, the stability boundary characterization for layered stars exhibits a slight offset from the traditional BTM criteria [59] in the M - R relation, according to the radial mode results calculated in [7]. For mixed-core models, the stability analysis is more complex, and their manifestation in macroscopic quantities must satisfy a generalization of the BTM criteria, which will be discussed in the next sections. In the following, we focus on this mixed star case, which is the scenario II in Fig.1.

B. Equilibrium Configuration

The commonly used model for describing compact star equilibrium configuration is provided by the TOV formalism. This framework comprises a set of differential equations for a static, non-rotating star modeled as an ideal fluid in spherical symmetry.

Based on a spherically symmetric metric line element with Schwarzschild-like coordinates (t, r, θ, ϕ) ,

$$ds^2 = -e^{2\phi(r)}c^2dt^2 + \left(1 - \frac{2Gm(r)}{rc^2}\right)^{-1}dr^2 + r^2d\Omega^2, \quad (1)$$

where $d\Omega^2 = d\theta^2 + \sin^2\theta d\phi^2$, and the energy-momentum tensor for an ideal fluid

$$T^{\mu\nu} = (\rho(1 + \zeta/c^2) + p/c^2)u^\mu u^\nu + pg^{\mu\nu}, \quad (2)$$

with p the fluid pressure, ζ the specific energy density, ρ the rest mass density, and u^μ the four-velocity vector. The TOV equations can be derived by substituting them into the Einstein equation

$$G^{\mu\nu} = \frac{8\pi G}{c^4}T^{\mu\nu}, \quad (3)$$

together with the energy-momentum conservation

$$\nabla T^{\mu\nu} = 0. \quad (4)$$

The explicit TOV equations are given as follows:

$$\begin{aligned} \frac{dp}{dr} &= -G(\rho(r)(1 + \zeta(r)/c^2) + p(r)/c^2) \\ &\quad \frac{m(r) + 4\pi r^3 p(r)/c^2}{r(r - 2Gm(r)/c^2)}, \\ \frac{dm}{dr} &= 4\pi r^2 \rho(r)(1 + \zeta(r)/c^2), \\ \frac{d\phi}{dr} &= \frac{m(r) + 4\pi r^3 p(r)/c^2}{r(r - 2Gm(r)/c^2)}, \end{aligned} \quad (5)$$

where $m(r)$ is the gravitational mass within radius r .

Defining the total energy density as $\varepsilon = \rho c^2 + \rho\zeta$ and adopting the natural unit system, we simplify (5) to

$$\begin{aligned} \frac{dp}{dr} &= -(\varepsilon(r) + p(r)) \frac{m(r) + 4\pi r^3 p(r)}{r(r - 2m(r))}, \\ \frac{dm}{dr} &= 4\pi r^2 \varepsilon(r), \\ \frac{d\phi}{dr} &= \frac{m(r) + 4\pi r^3 p(r)}{r(r - 2m(r))}. \end{aligned} \quad (6)$$

We adopt the equations (6) in our subsequent single-fluid numerical calculations.

The boundary conditions are prescribed as follows: at the star center, the mass within an infinitesimal radius must approach zero; at the surface (where $r = R$, with R denoting the star radius), the metric potential ϕ assumes its vacuum form, $\phi = \frac{1}{2} \ln(1 - 2GM/(Rc^2))$, which matches the Schwarzschild exterior solution, where $M \equiv m(R)$ represents the total mass enclosed within the star radius. The central pressure $p_c \equiv p(0)$, on the other hand, serves as a free parameter that may be specified independently.

While the above TOV equations typically models the interior of a compact star as an ideal fluid composed of a single species of matter, the physical scenario under consideration here is more complex: a DM/NM mixed star. Generally, models with multiple matter components can be constructed using either a single-fluid approximation [60][61] (where the system is still treated as one effective fluid, but with an EoS incorporating contributions from multiple components) or a multi-fluid formalism (where distinct matter components are described by separate EoS). In the case of a weakly coupled multi-fluid model with only gravitational interactions—meaning the energy-momentum tensors of the individual components are decoupled—it is possible to derive a multi-fluid gen-

eralization of the TOV equation [11, 62]:

$$\begin{aligned}\frac{dp_I}{dr} &= -(\varepsilon_I(r) + p_I(r)) \frac{m_t(r) + 4\pi r^3 p_t(r)}{r(r - 2m_t(r))}, \\ \frac{dm_I}{dr} &= 4\pi r^2 \varepsilon_I(r), \\ \frac{d\phi}{dr} &= \frac{m_t(r) + 4\pi r^3 p_t(r)}{r^2 \left(1 - \frac{2m_t(r)}{r}\right)},\end{aligned}\quad (7)$$

where the subscript I indicates the components of the substance. $m_t = \sum_I m_I$, $p_t = \sum_I p_I$ and $\varepsilon_t = \sum_I \varepsilon_I$ are the sums of respective quantities from contributions of each fluid component. When p_I reaches zero, the corresponding radius and mass for that component are R_I and M_I . When p_t reaches zero, we have the total star radius R_t , and the total star mass $M = \sum_I M_I$.

In addition to the nature units, we further apply astrophysical units for later convenience. The units of mass, pressure, energy density and radius are M_\odot , $p_\odot = \varepsilon_\odot = 1/M_\odot^2$, and km, respectively, where M_\odot denotes the solar mass.

C. Equation of State

There are many existing EoS models of NS and quark stars, such as FPS [63], APR (ALF) [64], WFF [65], MPA1 [66], MSL [67], H4, [68] and the BSK family of models [69].

To check the stability, we can deal with all kinds of EoS, either numerical or analytical. In our project, we take one numerical EoS and three analytical EoS for example.

For NS EoS, we first consider the famous SLy4 [70–72], which survives from the GW170817 [1] and NICER [73] observation constraints. It is a Skyrme-type effective nuclear interaction parametrization, tailored for describing asymmetric NM. Its parameters are derived by fitting to microscopic NM calculations and experimental data of doubly magic nuclei, achieving self-consistency between nuclear and NS physics. However it has many adjustable parameters and doesn't have an analytic form.

The second is a double-polytropic EoS [74] derived from AdS/QCD and the Witten-Sakai-Sugimoto model [75, 76], by introducing an instanton gas structure in D-brane background and solving the free energy variational equations. This model could only support a maximum mass of $1.85M_\odot$, but can still work as a good reference since it is in a general analytical form, which is easy to be altered to other situations:

$$\varepsilon = 0.140\mathcal{A}^{0.571}p^{0.429} + 3.896\mathcal{A}^{-0.335}p^{1.335}, \quad (8)$$

where $\mathcal{A} = 1.8 \times 10^{-5} \times \ell^{-7}$, and ℓ (brane asymptotic separation) is the only adjustable parameter. We refer this EoS as Holographic EoS later.

For the DM component in mixed stars, the EoS is determined by the chosen DM model. Studies have employed free Fermi gas DM combined with the SLy4 NS

model to investigate mixed star stability [19]. In this work, we also include this EoS for comparison. The EoS for such free Fermionic DM is given by [77, 78]:

$$\begin{aligned}\varepsilon &= \frac{1}{2\pi^2} \int_0^{k_F} dk k^2 \sqrt{k^2 + m_f^2} \\ &= \frac{1}{8\pi^2} \left[k_F \sqrt{k_F^2 + m_f^2} (2k_F^2 + m_f^2) \right. \\ &\quad \left. - m_f^4 \ln \left(\frac{k_F + \sqrt{k_F^2 + m_f^2}}{m_f} \right) \right], \\ p &= \frac{1}{6\pi^2} \int_0^{k_F} dk \frac{k^4}{\sqrt{k^2 + m_f^2}} \\ &= \frac{1}{24\pi^2} \left[k_F \sqrt{k_F^2 + m_f^2} (2k_F^2 - 3m_f^2) \right. \\ &\quad \left. + 3m_f^4 \ln \left(\frac{k_F + \sqrt{k_F^2 + m_f^2}}{m_f} \right) \right],\end{aligned}\quad (9)$$

where m_f is the fermion mass and k_F is the Fermi momentum. Various interactions can be incorporated into this free Fermi gas model to construct more sophisticated EoS.

For Bosonic DM, a stable mixed star model cannot be formed with free bosons due to the absence of degeneracy pressure. Given the weak interaction between DM and NM, it is natural to consider self-interacting bosonic DM to construct the DM EoS that balances the self-gravitational effect. In this project, we utilize a scalar field theory with the potential $V(\phi) = \frac{m_b^2}{2} |\phi|^2 + \frac{\lambda_4}{4} |\phi|^4$, as proposed in [79], where m_b is the boson mass and λ_4 is the coupling. In the isotropic limit, this theory yields the following EoS [34]:

$$\varepsilon = 3p + B\sqrt{\varepsilon}, \quad (10)$$

where the free parameter is $B = \frac{0.08}{\sqrt{\lambda_4}} \left(\frac{m}{\text{GeV}}\right)^2$.

III. STABILITY CRITERIA

In the previous section, we obtained the method for determining the equilibrium structure of compact stars. Using this method, the distributions of the star's physical properties—including pressure, energy density, mass, and particle number density (which will be discussed later)—can be uniquely determined by the central pressure. However, such equilibrium solutions may correspond to either stable or unstable configurations. In practical applications, we are typically only concerned with stable configurations. To determine the stability of an equilibrium configuration, it is further required to compute the frequencies its normal modes under radial perturbations.

In addition to rigorously determining star stability through such solutions, BTM criteria is an alternative method, which determines the stability of single-fluid compact stars using solely equilibrium configuration solutions. This approach is more intuitive and computationally efficient.

For multi-fluid stars, the work of Henriques et al. [8] as well as other works such as [80][19] adopted another method based on mass-particle number relation in configuration sequence to identify the critical points between stability and instability. In this section, we will introduce both the method for computing radial oscillation modes for single- and two-fluid stars and the method for directly determining stability using equilibrium solutions. Furthermore, we will rigorously demonstrate the equivalence of these two stability criteria based on the variational principles and the covariant conservation law.

A. Radial Oscillation

1. Single Fluid

Chandrasekhar, in his 1964 paper, rigorously established the pulsation equation for radial oscillations in single-fluid stars based on radial perturbations and variational principles [2], and it is widely applied in many works such as [81]. For the need of unifying notation, we briefly review the main steps and key equations in the derivation of this equation:

Linearization of the Field Equations

An unperturbed, static, spherically symmetric equilibrium configuration is assumed, satisfying the TOV equations. Its behavior after being subjected to infinitesimal radial perturbations can be used to determine its stability. We define $e^{2\lambda(r)} \equiv \left(1 - \frac{2Gm(r)}{rc^2}\right)^{-1}$, then the metric and fluid variables are written as:

$$\begin{aligned}\lambda &= \lambda_0 + \delta\lambda, & \phi &= \phi_0 + \delta\phi, \\ p &= p_0 + \delta p, & \varepsilon &= \varepsilon_0 + \delta\varepsilon.\end{aligned}$$

The Einstein field equations and the Einstein-Euler equations are perturbed separately. Neglecting higher-order terms, we obtain the corresponding system of linearized

radial perturbation equations:

$$\frac{\partial}{\partial r}(re^{-2\lambda_0}\delta\lambda) = \frac{4\pi G}{c^4}r^2\delta\varepsilon, \quad (11)$$

$$\frac{e^{-2\lambda_0}}{r} \left(\frac{\partial}{\partial r}\delta\phi - \frac{2d\phi_0}{dr}\delta\lambda \right) = \frac{e^{-2\lambda_0}}{r^2}\delta\lambda + \frac{4\pi G}{c^4}\delta p, \quad (12)$$

$$\frac{e^{-2\lambda_0}}{r} \frac{\partial}{\partial t}\delta\lambda = -\frac{4\pi G}{c^4}(p_0 + \varepsilon_0)\frac{dr}{dt}, \quad (13)$$

$$\begin{aligned}e^{2\lambda_0-2\phi_0}(p_0 + \varepsilon_0)\frac{\partial}{\partial t}\frac{dr}{dt} + \frac{\partial}{\partial r}\delta p + \\ (p_0 + \varepsilon_0)\frac{\partial}{\partial r}\delta\phi + (\delta p + \delta\varepsilon)\frac{d\phi_0}{dr} = 0.\end{aligned} \quad (14)$$

Lagrangian Displacement and Reformulating Perturbations

The *Lagrangian displacement* ξ is defined such that the radial velocity satisfies $v = \frac{dr}{dt} = \frac{\partial\xi}{\partial t}$, i.e., $u^r = e^{-\phi_0}\frac{dr}{dt} = e^{-\phi_0}\frac{\partial\xi}{\partial t}$. Then, using the first three equations of the linearized perturbation equations (11)(12)(13), all perturbations of metric and fluid variables except δp are expressed in terms of ξ and equilibrium quantities:

$$\delta\lambda = -\frac{4\pi G}{c^4}\xi(p_0 + \varepsilon_0)\frac{r}{e^{-2\lambda_0}}, \quad (15)$$

$$\delta\varepsilon = -\frac{1}{r^2}\frac{\partial}{\partial r}\left[r^2(p_0 + \varepsilon_0)\xi\right], \quad (16)$$

$$\frac{\partial}{\partial r}\delta\phi = \frac{4\pi G}{c^4}\left[\delta p - (p_0 + \varepsilon_0)\left(\frac{2d\phi_0}{dr} + \frac{1}{r}\right)\xi\right]\frac{r}{e^{-2\lambda_0}}. \quad (17)$$

Note that the perturbation quantities and the Lagrangian displacement are all functions of r and t (e.g., $\xi(r, t)$, $\delta p(r, t)$, etc.). We now assume that all perturbation quantities F possess a time-harmonic dependence of the form: $F(r, t) = F(r)e^{i\omega t}$. Based on this separation of variables and in combination of (14) with (15), (16), and (17), we obtain:

$$\begin{aligned}\omega^2 e^{2\lambda_0-2\phi_0}(p_0 + \varepsilon_0)\xi = \\ -\frac{d\phi_0}{dr}(p_0 + \varepsilon_0)\frac{d\xi}{dr} \\ -\left[\frac{d\phi_0}{dr}\left(\frac{d(\varepsilon_0 + p_0)}{dr} + \frac{(p_0 + \varepsilon_0)}{r}\right) \right. \\ \left. + (p_0 + \varepsilon_0)\left(\frac{2d\phi_0}{dr} + \frac{1}{r}\right)\left(\frac{d\lambda_0}{dr} + \frac{d\phi_0}{dr}\right)\right]\xi \\ + \frac{d}{dr}\delta p + \delta p\frac{d}{dr}(\lambda_0 + 2\phi_0),\end{aligned} \quad (18)$$

where yet the perturbation equations are thus reduced from complex partial differential equations (PDE) to a relatively simpler eigenvalue problem governed by an ordinary differential equation (ODE), with the perturbation terms now consisting of only the pressure variation.

Baryon Number Conservation

An additional relation is needed to connect the pressure perturbation δp to the other variables. This is provided by imposing adiabaticity and baryon number conservation, which requires $\nabla_\mu(nu^\mu) = 0$. Defining the perturbation of n as $n = n_0(r) + \delta n(r, t)$ and combining it with ξ defined previously leads to the form of δn constituted by the Lagrangian displacement and the unperturbed terms:

$$\delta n = -\frac{e^{\phi_0}}{r^2} \frac{\partial(n_0 r^2 \xi e^{-\phi_0})}{\partial r}. \quad (19)$$

Moreover, the first law of thermodynamics gives $d\varepsilon = \frac{\varepsilon+p}{n} dn$, thus the baryon number density is now related to p or ε . This finally allows the pressure perturbation to be written solely in terms of the Lagrangian displacement:

$$\delta p = -\xi \frac{dp_0}{dr} - \gamma p_0 \frac{e^{\phi_0}}{r^2} \frac{\partial}{\partial r} (r^2 e^{-\phi_0} \xi). \quad (20)$$

Here γ is defined as $\gamma = -\frac{n_0}{p_0} \frac{dp_0}{dn_0}$, which is the adiabatic index. This step is crucial as it incorporates the microphysics (EoS) into the dynamical description.

The Pulsation Equation and Boundary Conditions

Substituting the expression for the pressure perturbation δp from (20) into the perturbed equation of motion (18), and after involving the use of the background TOV equations (6) to eliminate derivatives of the metric potentials, one arrives at the final pulsation equation:

$$\begin{aligned} \omega^2 e^{2(\lambda_0 - \phi_0)} (p_0 + \varepsilon_0) \xi &= \frac{4}{r} \frac{dp_0}{dr} \xi \\ &- e^{-(\lambda_0 + 2\phi_0)} \frac{d}{dr} \left[e^{(\lambda_0 + 3\phi_0)} \frac{\gamma p_0}{r^2} \frac{d}{dr} (r^2 e^{-\phi_0} \xi) \right] \\ &+ \frac{8\pi G}{c^4} e^{2\lambda_0} p_0 (p_0 + \varepsilon_0) \xi \\ &- \frac{1}{p_0 + \varepsilon_0} \left(\frac{dp_0}{dr} \right)^2 \xi. \end{aligned} \quad (21)$$

To cast it into the standard Sturm-Liouville form, we need two key simplifications: multiplying the entire equation (21) by $e^{\lambda_0 + 2\phi_0}$ to simplify the differential operator and introducing the new variable $\chi(r) \equiv r^2 e^{-\phi_0(r)} \xi(r)$ to simplify the expression for the Lagrangian perturbation. After manipulation, the equation takes the canonical Sturm-Liouville form:

$$-\frac{d}{dr} \left[P(r) \frac{d\chi}{dr} \right] + Q(r) \chi = \omega^2 W(r) \chi, \quad (22)$$

where the coefficient functions are defined as:

$$\begin{aligned} P(r) &= \frac{\gamma p_0(r)}{r^2} e^{\lambda_0(r) + 3\phi_0(r)}, \\ Q(r) &= \left(\frac{4}{r} \frac{dp_0}{dr} + \frac{8\pi G}{c^4} e^{2\lambda_0(r)} p_0(r) (p_0(r) + \varepsilon_0(r)) \right. \\ &\quad \left. - \frac{1}{p_0(r) + \varepsilon_0(r)} \left(\frac{dp_0}{dr} \right)^2 \right) \frac{e^{\lambda_0(r) + 3\phi_0(r)}}{r^2}, \\ W(r) &= (p_0(r) + \varepsilon_0(r)) \frac{e^{3\lambda_0 + \phi_0}}{r^2}. \end{aligned}$$

This formulation demonstrates the self-adjoint nature of the eigenvalue problem, which guarantees real eigenvalues ω^2 as well as orthogonal and complete eigenfunctions.

Solutions to the pulsation equation must satisfy boundary conditions imposed by physical regularity and spherical symmetry:

- At the center of the star ($r = 0$), all physical quantities must be finite. The radial displacement ξ must vanish at the origin to avoid a directional singularity, i.e., $\xi(0) = 0$. A power series analysis shows that the leading-order of the displacement is linear: $\xi \propto r$. Thus, due to the factor of r^2 , the scaling variable $\chi(r) = r^2 e^{-\phi_0(r)} \xi(r)$ has an asymptotic behavior $\chi \propto r^3$ near the origin. Therefore, the inner boundary condition is:

$$\chi \rightarrow 0 \quad \text{as} \quad r \rightarrow 0, \quad \text{with} \quad \frac{\chi}{r^3} \rightarrow \text{const.} \quad (23)$$

In practice, for numerical integration, this is implemented by starting the integration at a small but finite radius $r = r_0$ with the asymptotic form $\chi(r_0) = \chi_0 r_0^3$, where χ_0 is a constant to be determined.

- At the surface of the star, the appropriate physical boundary condition is that the Lagrangian perturbation of the pressure must vanish:

$$\Delta p = 0 \quad \text{at} \quad r = R. \quad (24)$$

And its relation to the Eulerian perturbation is:

$$\begin{aligned} \Delta p &= \delta p + \xi \frac{dp_0}{dr} \\ &= -\gamma p_0 \frac{e^{\phi_0}}{r^2} \frac{\partial}{\partial r} (r^2 e^{-\phi_0} \xi), \end{aligned} \quad (25)$$

Therefore, in numerical calculations, we require that the right side of IIIA should be zero on the outer boundary.

The pulsation equation in Sturm-Liouville form, together with the boundary conditions (23) and (24), defines a characteristic value problem for the squared oscillation frequency ω^2 .

Stability Condition and Variational Principle

The stability of an equilibrium configuration is determined by the temporal evolution of radial perturbations. From the ansatz $\xi(r, t) = \xi(r)e^{i\omega t}$, real values of ω (i.e., $\omega^2 > 0$) correspond to stable oscillations, while imaginary ω ($\omega^2 < 0$) leads to exponentially growing or damping modes, indicating dynamical instability.

The self-adjoint nature of the pulsation equation (21) permits the formulation of a variational principle for the characteristic frequencies ω^2 . Multiplying (21) by $r^2 \xi e^{(-\phi_0)}$ and integrating over the star volume, followed by integration by parts and application of the boundary conditions, yields the integral expression:

$$\omega^2 \int_0^R e^{(3\lambda_0 - \phi_0)} (p_0 + \varepsilon_0) r^2 \xi^2 dr = \text{Numerator}, \quad (26)$$

where the right-hand side “Numerator” is given by the integral:

$$\begin{aligned} \text{Numerator} = & 4 \int_0^R e^{(\lambda_0 + \phi_0)} r \frac{dp_0}{dr} \xi^2 dr \\ & + \int_0^R e^{(\lambda_0 + 3\phi_0)} \frac{\gamma p_0}{r^2} \left[\frac{d}{dr} (r^2 e^{-\phi_0} \xi) \right]^2 dr \\ & - \int_0^R e^{(\lambda_0 + \phi_0)} \left(\frac{dp_0}{dr} \right)^2 \frac{r^2 \xi^2}{p_0 + \varepsilon_0} dr \\ & + \frac{8\pi G}{c^4} \int_0^R e^{(3\lambda_0 + \phi_0)} p_0 (p_0 + \varepsilon_0) r^2 \xi^2 dr. \end{aligned} \quad (27)$$

Equation (26) expresses ω^2 as the ratio of two integrals, known as the *Rayleigh quotient*:

$$\begin{aligned} \omega^2[\xi] &= \frac{\text{Numerator}}{\text{Denominator}}, \\ \text{where} \quad & \\ \text{Denominator} &= \int_0^R e^{(3\lambda_0 - \phi_0)} (p_0 + \varepsilon_0) r^2 \xi^2 dr. \end{aligned} \quad (28)$$

Here, $\omega^2[\xi]$ is a functional, whose value depends on the choice of the trial function ξ .

The orthogonality of the eigenfunctions, as guaranteed by the self-adjoint Sturm-Liouville form, plays a crucial role in the variational principle. Any admissible trial function ξ can be expanded as a series in the complete set of orthogonal eigenfunctions $\xi^{(n)}$:

$$\tilde{\xi} = \sum_{n=0}^{\infty} c_n \xi^{(n)}, \quad (29)$$

where c_n is the weight coefficients. The functional $\tilde{\omega}^2[\tilde{\xi}]$ corresponding to the trial function is a weighted average of the true eigenvalues ω_n^2 :

$$\tilde{\omega}^2 = \frac{\sum_{n=0}^{\infty} c_n^2 \omega_n^2 \langle \xi^{(n)}, \xi^{(n)} \rangle}{\sum_{n=0}^{\infty} c_n^2 \langle \xi^{(n)}, \xi^{(n)} \rangle}, \quad (30)$$

where $\langle \cdot, \cdot \rangle$ denotes the inner product with the corresponding weight functions. The Rayleigh quotient is stationary when $\tilde{\xi}$ is an eigenfunction (see more details in [82]), and attains its minimum value ω_0^2 when $\tilde{\xi}$ is proportional to the fundamental mode $\xi^{(0)}$.

Therefore, for any trial function $\tilde{\xi}$ satisfying the boundary conditions, the computed value $\tilde{\omega}^2$ is an upper bound to the true fundamental mode eigenvalue:

$$\omega_0^2 \leq \tilde{\omega}^2[\tilde{\xi}]. \quad (31)$$

This formulation provides a powerful method for determining dynamical stability. A sufficient condition for dynamical instability is that there exists *any* trial function $\tilde{\xi}$ for which the “Numerator” ≤ 0 . Since the “Denominator” is always positive, this implies $\tilde{\omega}^2 \leq 0$, and consequently, $\omega_0^2 \leq 0$.

2. Multi-Fluid

For a compact star composed of multiple ideal fluids that are in the absence of any non-gravitational coupling, the pulsation equations for a single fluid can be generalized to the multi-fluid case. The oscillation equations for such a system have been previously derived in the literature and applied to other mixed models (see, e.g., [[18][19][83]]). This section briefly outlines the main steps in deriving the equations using the same process as the last text.

Linearized Field Equations and Energy-Momentum Tensor

Consider a spherically symmetric system composed of \mathcal{N} ideal fluids. The total energy-momentum tensor is the sum of the decoupled contributions from each fluid:

$$T_{\text{total}}^{\mu\nu} = \sum_I T_I^{\mu\nu}, \quad T_I^{\mu\nu} = (\varepsilon_I + p_I) u_I^\mu u_I^\nu + p_I g^{\mu\nu}.$$

For a spherically symmetric background, assuming the EoS for each fluid depends only on its own energy density (i.e., the fluids only interact through gravity): $p_I = p_I(\varepsilon_I)$, the radial perturbation variables are set as

$$\begin{aligned} \phi &= \phi_0 + \delta\phi, \quad \lambda = \lambda_0 + \delta\lambda, \\ \varepsilon_I &= \varepsilon_{I0} + \delta\varepsilon_I, \quad p_I = p_{I0} + \delta p_I, \end{aligned}$$

and the Lagrangian displacement ξ_I of the I -th fluid satisfies $v_I = \dot{\xi}_I$. Similar to the case of a single fluid, linearizing the Einstein field equations and the energy-momentum conservation equations would yield a set of coupled perturbation equations.

Lagrangian Displacement and Expression of Perturbations

Introduce the harmonic time dependence assumption: $\xi_I(t, r) = \xi_I(r)e^{i\omega t}$, and similarly for other perturbation

variables. Similar to the last section, the metric perturbations $\delta\lambda$, $\delta\phi$ can be expressed in terms of the time-independent ξ_I :

$$\delta\lambda = \frac{-8\pi Gr}{e^{-2\lambda_0}} \sum_I (\varepsilon_{I0} + p_{I0}) \xi_I, \quad (32)$$

$$\frac{d\delta\phi}{dr} = \frac{2\left(\frac{d\phi_0}{dr} + \frac{d\lambda_0}{dr}\right)}{(\varepsilon_0^{\text{total}} + p_0^{\text{total}})} \times \left[\delta p^{\text{total}} - \left(2\frac{d\phi_0}{dr} + \frac{1}{r}\right) \sum_I (\varepsilon_{I0} + p_{I0}) \xi_I \right]. \quad (33)$$

The energy density perturbation of each fluid can be written as:

$$\delta\varepsilon_I = -\frac{1}{r^2} \frac{\partial [r^2(p_{I0} + \varepsilon_{I0})\xi_I]}{\partial r} + \frac{4\pi G}{e^{-2\lambda_0}} (\varepsilon_{I0} + p_{I0}) r \sum_J (\varepsilon_{J0} + p_{J0}) (\xi_J - \xi_I). \quad (34)$$

Particle Number Conservation and Pressure Perturbation

Similar to the case of a single fluid, through covariant conservation, particle number perturbations are constructed as

$$\delta n_I = -\frac{e^{\phi_0}}{r^2} \frac{\partial (r^2 e^{-\phi_0} n_{I0} \xi_I)}{\partial r} + \frac{4\pi Gr}{e^{-2\lambda_0}} n_{I0} \sum_J (\varepsilon_{J0} + p_{J0}) (\xi_J - \xi_I). \quad (35)$$

For each fluid, introduce the adiabatic index $\gamma_I = -\frac{n_{I0}}{p_{I0}} \frac{dp_{I0}}{dn_{I0}} = \left(\frac{p_{I0} + \varepsilon_{I0}}{p_{I0}}\right) \frac{dp_{I0}}{d\varepsilon_{I0}}$. The pressure perturbation can then be expressed as:

$$\delta p_I = -\xi_I \frac{\partial p_{I0}}{\partial r} - \gamma_I p_{I0} \left[\frac{e^{\phi_0}}{r^2} \frac{\partial}{\partial r} (r^2 e^{-\phi_0} \xi_I) - \frac{4\pi Gr}{e^{-2\lambda_0}} \sum_J (\varepsilon_{J0} + p_{J0}) (\xi_J - \xi_I) \right]. \quad (36)$$

These perturbation expressions couple the fluid variables and the displacements ξ_I of all fluids, reflecting the gravitational interaction between the multiple fluids.

Multi-fluid Pulsation Equations and Boundary Conditions

Substituting the above expressions into the linearized equations and introducing the variable $\chi_I(r) = r^2 e^{-\phi_0} \xi_I(r)$ (where $\phi_c = \phi_0$ ($r=0$)) yield a set of coupled second-order ordinary differential equations:

$$\partial_r (P_I \chi_I') + (Q_I + \omega^2 W_I) \chi_I + \text{coupling terms} = 0, \quad (37)$$

where the coefficients are:

$$\begin{aligned} P_I &= \frac{1}{r^2} p_{I0} \gamma_I e^{2\phi_0}, \\ W_I &= \frac{1}{r^2} (\varepsilon_{I0} + p_{I0}) e^{2\lambda_0}, \\ Q_I &= -\frac{e^{2\phi_0}}{r^2} \left[\frac{3}{r} \frac{dp_{I0}}{dr} + 8\pi e^{2\lambda_0} p_0^{\text{total}} (\varepsilon_{I0} + p_{I0}) + e^{2\lambda_0} \left(4\pi r \varepsilon_0^{\text{total}} - \frac{m_0^{\text{total}}}{r^2} \right) \left(\frac{\varepsilon_{I0} + p_{I0}}{r} - \frac{dp_{I0}}{dr} \right) \right]. \end{aligned}$$

The coupling terms are explicitly given by:

coupling terms =

$$\begin{aligned} &R \left[\left(\frac{\varepsilon_{I0} + p_{I0}}{r} - \frac{dp_{I0}}{dr} \right) \sum_J (\varepsilon_{J0} + p_{J0}) \chi_J + \frac{r^2 (\varepsilon_{I0} + p_{I0})}{e^{2\phi_0}} \sum_J \left(p_{J0} \gamma_J \frac{e^{2\phi_0}}{r^2} \frac{d\chi_J}{dr} \right) \right] \\ &+ S_I \sum_J (\varepsilon_{J0} + p_{J0}) (\chi_J - \chi_I) \\ &+ \frac{r^2}{e^{2\phi_0}} R^2 (\varepsilon_{I0} + p_{I0}) \\ &\sum_J \sum_K p_{J0} \gamma_J (\varepsilon_{K0} + p_{K0}) (\chi_K - \chi_J) \\ &+ R \gamma_I p_{I0} \sum_J [(\varepsilon_{J0}' + p_{J0}') (\chi_J - \chi_I) + (\varepsilon_{J0} + p_{J0}) \left(\frac{d\chi_J}{dr} - \frac{d\chi_I}{dr} \right)], \end{aligned}$$

where

$$\begin{aligned} R &= 4\pi e^{2\lambda_0 + 2\phi_0} / r, \\ S_I &= R \left[(\gamma_I - 1) \frac{dp_{I0}}{dr} + \frac{d\gamma_I}{dr} p_{I0} + \gamma_I p_{I0} \left(8\pi r e^{2\lambda_0} (\varepsilon_0^{\text{total}} + p_0^{\text{total}}) - \frac{1}{r} \right) \right]. \end{aligned}$$

The boundary conditions are as follows:

- At the star center ($r=0$), $\chi_I \propto r^3$ for each fluid.
- At the boundary of each fluid $r = R_I$, the Lagrangian pressure perturbation must vanish, i.e.,

$$\begin{aligned} \Delta p_I &= \delta p_I + \xi_I \frac{dp_{I0}}{dr} \\ &= -\xi_I \frac{dp_{I0}}{dr} + \xi_I \frac{dp_{I0}}{dr} \\ &\quad - \gamma_I p_{I0} \left[\frac{e^{\phi_0}}{r^2} \frac{\partial}{\partial r} (r^2 e^{-\phi_0} \xi_I) - \frac{4\pi Gr e^{2\lambda_0}}{e^{-2\lambda_0}} \sum_J (\varepsilon_{J0} + p_{J0}) (\xi_J - \xi_I) \right] \\ &= 0. \end{aligned} \quad (38)$$

Among this, p_{I0} tends to 0 at the corresponding outer boundary of the fluid. Therefore, since the other quantities (ξ_I and unperturbed quantities) in the last term must be finite, the contribution of this term to the boundary constraint is ignored, and thus the boundary condition reduces to

$$\Delta p_I = -\gamma_I p_{I0} \left[\frac{e^{\phi_0}}{r^2} \frac{\partial}{\partial r} (r^2 e^{-\phi_0} \xi_I) \right] = 0. \quad (39)$$

This outer boundary condition is also consistent with those in [56, 82]. In [18] the corresponding term of e^{ϕ_0} is $e^{2\phi_0}$ after unifying the convention, which seems to be typo. But this slight discrepancy merely introduces a negligible scaling factor in the numerical results and does not affect the stability boundary.

Stability Condition and Variational Principle

The same stability criterion from the single-fluid analysis carries over to the two-fluid case: for perturbations of the form $\xi_I(r, t) = \xi_I(r) e^{i\omega t}$, the configuration is stable for real ω and dynamically unstable for imaginary ω .

Although the multi-fluid pulsation equations cannot be written in a standard Sturm-Liouville form, one can still give the coupled Rayleigh quotient:

$$\omega^2[\{\xi_I\}] = \frac{\text{Denominator}[\{\xi_I\}]}{\text{Numerator}[\{\xi_I\}]},$$

which could be constructed by the integration of the pulsation equation, including various complex coupling terms. The extreme value of its trial functions are the eigenvalues, and the minimum value is the square of the fundamental frequency. If there exists a set of trial functions $\{\tilde{\xi}_I\}$ such that $\omega^2 < 0$, then the system is unstable to that perturbation mode.

B. Critical Point/Curve Criteria

The stability criteria introduced in this section rely on examining the properties of the entire equilibrium sequence curve/surface (such as extremum points of mass). Relying on such criteria, one cannot determine stability based on a single isolated configuration; instead, its position within the entire sequence must be considered. Therefore, if the complete sequence has already been computed, applying these methods to analyze stability is convenient and essentially "free" and requires no additional calculations.

1. BTM Criteria for Single-Fluid

The BTM criteria is a method for assessing the radial stability of general relativistic star models. The key prin-

ciples of this criterion are (we apply its generalized version in [54], that when passing through each extremum of the M - R curve, the direction can go along either increasing or decreasing the core pressure):

- Stability changes occur exclusively at the extrema of the M - R curve.
- A **counterclockwise bend** at an extremum corresponds to **gaining one unstable mode**.
- A **clockwise bend** at an extremum corresponds to **losing one unstable mode**.
- The sequence is typically parameterized by central pressure.

It is crucial to emphasize that the original BTM criteria was formulated specifically for sequences of **zero-temperature stars**, representing a "family" of different stars composed of the same cold matter. This framework is directly applicable to the cold NS models considered in this work. In contrast, for sequences of **hot isentropic stars** with a fixed total baryon number, the stability change at an extremum follows the opposite rule [59]: a counterclockwise bend leads to the loss of an unstable mode, while a clockwise bend leads to the gain of one.

Due to its intuitive nature, the BTM criteria has been widely used for decades as a primary tool for stability assessment in relativistic astrophysics. The equivalence between the oscillation method and BTM criteria has been proved in [84, 85].

It is important to note that the BTM criteria is specifically applicable to **single-fluid models** and becomes invalid for **multi-fluid models** containing interface or mixed phases. We will provide a more detailed discussion of this fact and its manifestation in subsequent sections.

2. Critical Curve Criteria for Multi-Fluid

The stability analysis of multi-fluid compact stars can be significantly simplified through the application of the critical curve method. This approach, originally developed in [8] for determining the stability of boson-fermion stars, is in fact applicable to any spherically symmetric ideal multi-fluid star model in general relativity, including the DM-NM mixed stars considered in this work. The method provides an efficient criterion for determining star stability by relying solely on equilibrium solutions of the multi-fluid TOV equations, thereby circumventing the computationally intensive task of solving the coupled pulsation equations to identify radial normal modes.

The fundamental premise of this method lies in characterizing a stability boundary in the parameter space of central pressures for the constituent fluids. For a two-fluid system, the critical curve demarcating stable and unstable configurations is formed by a group of

points characterizing central conditions. At each point $\vec{\sigma} = (p_2^c, p_1^c)$, there exists a direction that fits the condition [8]:

$$\frac{dM(\infty)}{d\vec{\sigma}} = \frac{dN_F}{d\vec{\sigma}} \left(\text{or alternatively } \frac{dN_B}{d\vec{\sigma}} \right), \quad (40)$$

where $M(\infty)$ denotes the total gravitational mass of the star (equivalent to the mass within radius R , hereafter denoted simply as M) while N_F and N_B are the total particle numbers for fermions and bosons, respectively. For the specific case of DM-NM mixed stars considered in our work, this criterion takes the form:

$$\frac{dM}{d\vec{\sigma}} = \frac{dN_{NM}}{d\vec{\sigma}} \left(\text{or alternatively } \frac{dN_{DM}}{d\vec{\sigma}} \right), \quad (41)$$

where N_{NM} and N_{DM} represent the particle numbers of DM and NM, respectively.

In the subsequent section, we shall rigorously demonstrate a formal equivalence between the critical curve criterion and the traditional approach based on solving radial pulsation equations. This theoretical connection, though implicitly assumed in previous mixed star investigations, has rarely been explicitly established. We also have performed comprehensive numerical calculations applying both method to identical equation-of-state models within the same configuration space, validating the critical curve method as a reliable and efficient alternative for stability analysis in multi-fluid compact stars.

C. Equivalence

This section establishes the formal equivalence between the critical curve criterion introduced in Section III B and the traditional approach based on solving radial pulsation equations from Section III A.

Preliminary Remarks

Before proceeding to the equivalence proof, several important considerations must be emphasized:

1. **Stability vs. Zero-mode Condition:** The fundamental mode vanishing ($\omega_0^2 = 0$) represents a stronger condition than the existence of any zero-mode ($\exists n \in \mathbb{N} \text{ s.t. } \omega_n^2 = 0$). The critical curve method strictly identifies configurations where *some* mode has zero frequency. Additional verification is required to ensure that the curve corresponds to the fundamental mode.
2. **Model Assumptions and Mode Continuity:** For ideal fluids stars with fixed chemical composition and specific entropy, the dynamical equations are time-reversal invariant due to the absence of dissipative forces [86]. Consequently:

- Eigenvalues ω_n^2 vary continuously in the central pressure parameter space and this continuity guarantees that the critical curve properly separates stable and unstable regions

3. Mathematical Foundations: The existence of fundamental modes, the fact that the eigenvalues are real, and the completeness of mode expansions have been rigorously established by [82]. We adopt these conclusions without further proof.

Proof of Equivalence

The equivalence proof proceeds by establishing that the critical curve condition is equivalent to the existence of zero-frequency modes. We begin by reformulating the problem and then proceed through two main theorems.

In practical analysis, we identify the stability boundary critical curve as the locus of points where any two gradients among ∇M , ∇N_{NM} , and ∇N_{DM} become parallel. The equivalence we aim to prove can be formulated as:

$$\begin{aligned} (\nabla M \times \nabla N_{NM} = 0) \vee (\nabla M \times \nabla N_{DM} = 0) \\ \vee (\nabla N_{NM} \times \nabla N_{DM} = 0) \iff \exists n \text{ s.t. } \omega_n^2 = 0 \end{aligned} \quad (42)$$

We decompose this proof into two parts, demonstrating that both conditions are necessary and sufficient for:

$$\begin{aligned} (\nabla M \times \nabla N_{NM} = 0) \wedge (\nabla M \times \nabla N_{DM} = 0) \\ \wedge (\nabla N_{NM} \times \nabla N_{DM} = 0) \end{aligned} \quad (43)$$

a. Step 1: Zero Modes and parallel Condition we begin by proving the following theorem

Theorem III.1. *For a two-fluid equilibrium configuration, the three gradients, ∇M , ∇N_{NM} , and ∇N_{DM} , are mutually parallel if and only if there exists at least a zero mode respect to radial perturbation.*

Proof. If for a certain static equilibrium configuration, there exists $n \in \mathbb{N}$ such that $\omega_n^2 = 0$ (or almost zero, i.e., $\omega_n^2 \rightarrow 0^+$) under radial perturbation, the corresponding eigenmode becomes quasi-static, implying the existence of a perturbation normal mode that is almost time-independent, called a static solution:

$$\xi_{In}(r, t) = \xi_{In}(r)e^{-i\omega_n t} = \xi_{In}(r) \quad (44)$$

This perturbation mode signifies an infinitely slow translation between configurations $\vec{\sigma}$ and $\vec{\sigma} + \delta\vec{\sigma}$, where $\delta\vec{\sigma} = (\delta p_2^c, \delta p_1^c)$ corresponds to $\xi_{In}(r)$.

The connection between the existence of static solutions and the critical curve relies on conserved quantities. Recalling the derivation of the two-fluid equilibrium and oscillation equations, the definitions of the physical quantities and their perturbations in terms of

Lagrangian displacements originate from the covariant conservation equations of the energy-momentum tensor $\nabla_\mu T_I^{\mu\nu} = 0$ and the particle number density for each fluid $\nabla_\mu J_I^\mu = \nabla_\mu (n_I u_I^\mu) = 0$, and their perturbations. From this, we can directly conclude that the dynamical process corresponding to any perturbation mode of the radial oscillation equations for an equilibrium configuration conserves both total energy and particle number. The total energy here refers to the total energy of the star and its gravitational field, which corresponds to the gravitational mass M defined in our framework, equaling the sum of internal energy and rest mass energy:

$$M_{\text{total}} = E_{\text{internal}} + \sum_I m_{0I} N_I \quad (45)$$

where m_{0I} refers to fluid's single-particle mass.

We now explicitly verify this natural conclusion of particle number and total energy conservation:

- **Symbol definition: Conserved Charges and Currents**

We define the conserved charges and currents as Q_i and J_i^μ , $i = N_I, M_I$.

The conserved currents and charges are constructed as:

$$\begin{aligned} J_{N_I}^\mu &\equiv n_I u_I^\mu, \quad J_{M_I}^\mu \equiv T_I^{\mu 0}; \\ Q_i &\equiv - \int_\Sigma J_i^\mu a_\mu \sqrt{h} d^3x, \end{aligned} \quad (46)$$

where Σ is a spacelike hypersurface of fixed time, a_μ is the unit normal vector of Σ , h is the determinant of the induced 3-metric, and $\sqrt{h} d^3x$ is the invariant volume element on the 3-space.

Thus, Q_i represents the flux of J_i^μ through Σ .

- **Explicit Form of Conserved Charges**

Define $B = e^{2\phi}$, $A = e^{-2\nu}$. For $i = N_I$, the conserved charge is explicitly given by:

$$\begin{aligned} Q_{N_I} &= \int_\Sigma J_{N_I}^\mu a_\mu \sqrt{h} d^3x \\ &= \int_\Sigma J_{N_I}^0 \sqrt{B} \sqrt{h} d^3x \\ &= \int_\Sigma J_{N_I}^0 \sqrt{-g} d^3x \\ &= \int_\Sigma n_I u^0 r^2 \frac{\sqrt{B}}{\sqrt{A}} \sin\theta dr d\phi d\theta \\ &= \int_0^\infty 4\pi r^2 n_I u^0 \frac{\sqrt{B}}{\sqrt{A}} dr \\ &= \int_0^\infty 4\pi r^2 n_I \frac{1}{\sqrt{B}} \frac{\sqrt{B}}{\sqrt{A}} dr \\ &= \int_0^\infty 4\pi r^2 n_I \left(1 - \frac{2m_{\text{total}}}{r}\right)^{-\frac{1}{2}} dr \\ &= N_I. \end{aligned} \quad (47)$$

Similarly, for $i = M_I$:

$$\begin{aligned} Q_{M_I} &= \int_\Sigma J_{M_I}^\mu a_\mu \sqrt{h} d^3x = \int_\Sigma T_I^{00} \sqrt{-g} d^3x \\ &= \int_\Sigma \varepsilon_I \frac{\sqrt{A}}{\sqrt{B}} \sqrt{-g} d^3x = \int_0^\infty 4\pi r^2 \varepsilon_I dr = M_I. \end{aligned} \quad (48)$$

- **Covariant Conservation Law**

The covariant conservation law is given by:

$$\nabla_\mu J_i^\mu = 0.$$

- **Proof of Conservation**

Consider two adjacent spacelike hypersurfaces Σ_1 and Σ_2 , which together with a timelike boundary surface form a closed hypersurface. Since no current flows through the boundary, the flux of J_i^μ through the boundary vanishes.

The change in the conserved charge from Σ_1 to Σ_2 is equal to the total flux of J_i^μ through the closed hypersurface.

Applying the Stokes' theorem, this flux equals the volume integral of the covariant divergence of J_i^μ over the enclosed 4-volume:

$$\Delta Q_i = \int \nabla_\mu J_i^\mu \sqrt{-g} d^4x.$$

By the covariant conservation law $\nabla_\mu J_i^\mu = 0$, we obtain:

$$\Delta Q_i = 0,$$

which implies $\Delta N_I = 0$ and $\Delta M_I = 0$, thus proving the conservation of both charges.

Based on the above, we can conclude: if an equilibrium configuration possesses a radial normal mode with zero eigenvalue, then this mode corresponds to a static perturbation mode $\xi_{In}(r)$ which connects two neighboring equilibrium configurations while preserving both M and N_I . it follows that along this direction in parameter space, the total energy and particle numbers of each fluid must attain their extremal values:

$$\frac{dM_{\text{total}}}{d\vec{\sigma}} = 0 \quad \text{and} \quad \frac{dN_I}{d\vec{\sigma}} = 0, \forall I, \quad (49)$$

which is equivalent to the parallelism of the gradients of M and N_I :

$$\nabla M \parallel \nabla N_1 \parallel \nabla N_2, \quad (50)$$

where the symbol \parallel represents the parallel relation. \square

b. Step 2: Theorem 2 - Variational Extremum Principle The second part of the equivalence proof demonstrates that if any two of the three gradients ∇M , ∇N_{NM} , and ∇N_{DM} are parallel, then the third gradient is necessarily parallel to them as well. The detailed proof process is listed in the appendix A. In this section, we present the main steps:

Theorem III.2. *A two-fluid isentropic mixed star configuration satisfies the equilibrium equations if and only if the total mass M takes its extremal with respect to all time-independent variations that conserve the particle numbers of both fluids.*

Proof. We employ the method of Lagrange multipliers. The theorem statement is equivalent to the existence of Lagrange multipliers λ_1 and λ_2 such that the composite functional

$$H[\vec{\sigma}] = M[\vec{\sigma}] - \lambda_1 N_{NM}[\vec{\sigma}] - \lambda_2 N_{DM}[\vec{\sigma}] \quad (51)$$

is stationary with respect to arbitrary variations $\delta\epsilon_I(r)$.

The first order variation of the functional is:

$$\delta H = \delta M - \lambda_1 \delta N_{NM} - \lambda_2 \delta N_{DM}. \quad (52)$$

Applying the thermodynamic identity at zero temperature $\delta\epsilon_I = \mu_I \delta n_I = (\epsilon_I + p_I)/n_I \delta n_I$ (where μ_I is the chemical potential of fluid I) and converting particle density variations to energy density variations yields:

$$\delta H = \sum_{I=1,2} \int \left[\frac{\partial M}{\partial \epsilon_I} \delta \epsilon_I - \lambda_I \left(\frac{\partial N_I}{\partial \epsilon_I} \delta \epsilon_I + \sum_{J=1,2} \frac{\partial N_I}{\partial m_J} \delta m_J \right) \right] dr. \quad (53)$$

In order for this expression to be zero for any variation $\delta\epsilon_I(r)$, the integrated term must disappear, thus

$$\frac{\partial M}{\partial \epsilon_I} \delta \epsilon_I - \lambda_I \left(\frac{\partial N_I}{\partial \epsilon_I} \delta \epsilon_I + \sum_{J=1,2} \frac{\partial N_I}{\partial m_J} \delta m_J \right) = 0, \forall I. \quad (54)$$

For the existence of λ_1 and λ_2 holding the above equation true, we must impose constraints on the star configuration, which eventually leads to:

$$\frac{dp_I}{dr} = -(\epsilon_I + p_I) \frac{m_t + 4\pi r^3 p_t}{r(r - 2m_t)}, \quad (55)$$

for $I = DM, NM$,

which is exactly the first equilibrium equation (7) and the theorem is proved. \square

Since the Lagrange multipliers can be rescaled arbitrarily (for example, dividing $\nabla M = \lambda_1 \nabla N_{NM} + \lambda_2 \nabla N_{DM}$ by λ_1 or λ_2), the statement of this theorem remains valid under any permutation of M , N_{NM} , and N_{DM} . Because the arbitrary time-independent variations considered in the theorem apparently include the static perturbations corresponding to radial oscillation modes, this permutation symmetry implies that if any two of the three gradients (∇M , ∇N_{NM} , and ∇N_{DM}) are parallel (indicating

simultaneous extrema), the third must also be parallel to them. This reduces the requirement of mutual parallelism among all three gradients to the parallelism of any two gradients.

Physical Interpretation via Energy Considerations

For any equilibrium configuration, the stability with respect to radial perturbations can be assessed by the second-order variation of the total mass M . If the extremum of M (as defined in Theorem III.2) is a minimum, then the configuration is stable against radial perturbations; otherwise, it is unstable. This statement is equivalent to: the configuration is stable if $\delta^2 M$ is positive definite, otherwise (if there exists some perturbation such that $\delta^2 M < 0$), it is unstable.

For the non-rotating static zero-temperature two-fluid star model we consider, the following equivalence can be established within thermodynamic framework [82, 87, 88]: for a given linear perturbation mode $\xi = (\xi_1, \xi_2)$,

$$\text{sgn}(\delta^2 M[\xi]) = \text{sgn}(E_c[\xi]) = \text{sgn}(V[\xi]) = \text{sgn}(\omega_0^2), \quad (56)$$

where E_c and V are canonical energy and potential energy. The connection between their symbols and stability is:

- $\delta^2 M > 0 \Leftrightarrow \omega_0^2 > 0$: Stable configuration,
- $\delta^2 M = 0 \Leftrightarrow \omega_0^2 = 0$: Stability boundary,
- $\delta^2 M < 0$ (for some perturbation) $\Leftrightarrow \omega_0^2 < 0$: Unstable configuration.

The intuitive physical picture is as follows: $\delta^2 M > 0$ implies that any perturbation deviating from equilibrium increases the system's energy. By energy conservation, this energy must be supplied externally, indicating stability. Conversely, if $\delta^2 M < 0$, the perturbation could grow with kinetic energy without requiring external energy input, thus the steller is unstable.

IV. RESULTS

This section presents the numerical results of our investigation into the stability properties and macroscopic characteristics of mixed compact stars. We begin with a detailed stability analysis comparing single-fluid and multi-fluid models, followed by an examination of the resulting M - R relationships and their implications for astrophysical observations.

A. stability analyze

1. Single Fluid

As shown in Fig.3, we show the eigenvalue-central pressure relations for single-fluid models with three different

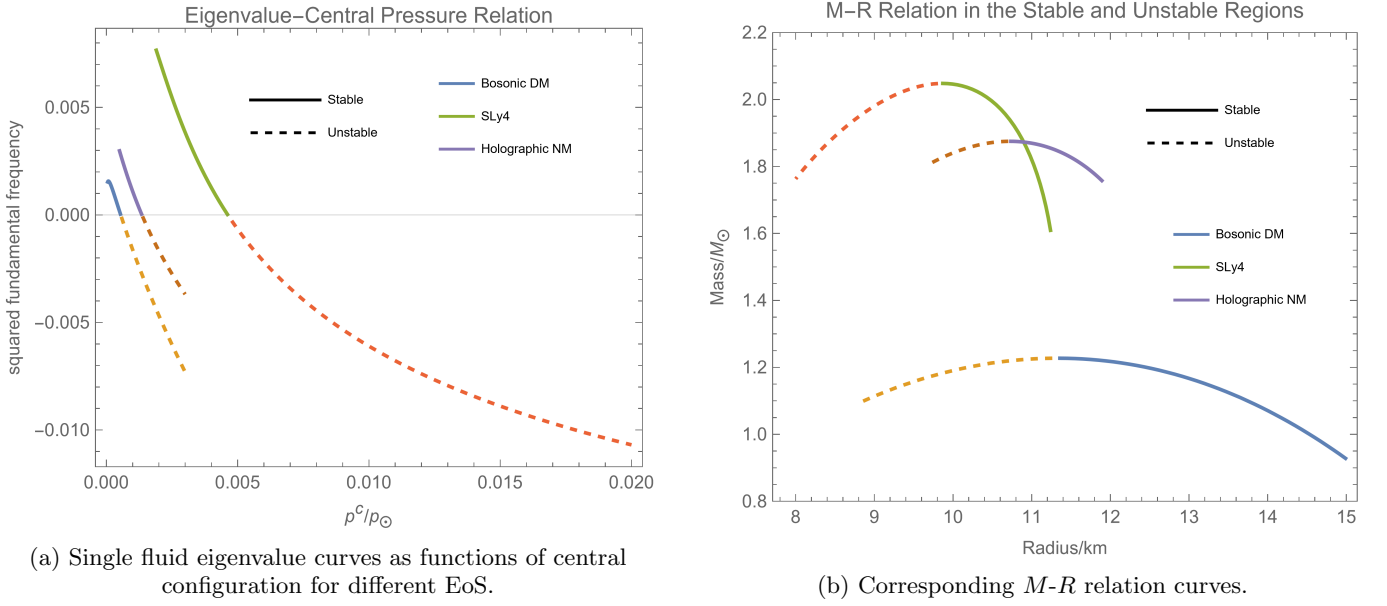


FIG. 3: Single fluid stability analysis. Left panel (Fig.3a) shows fundamental eigenvalue curves as functions of central configuration for different EoS: Bosonic DM ($B_4 = 0.1$), SLy4, and Holographic NM ($\ell^{-7} = 10300$) respectively. Right panel (Fig.3b) displays the corresponding M - R relation curves.

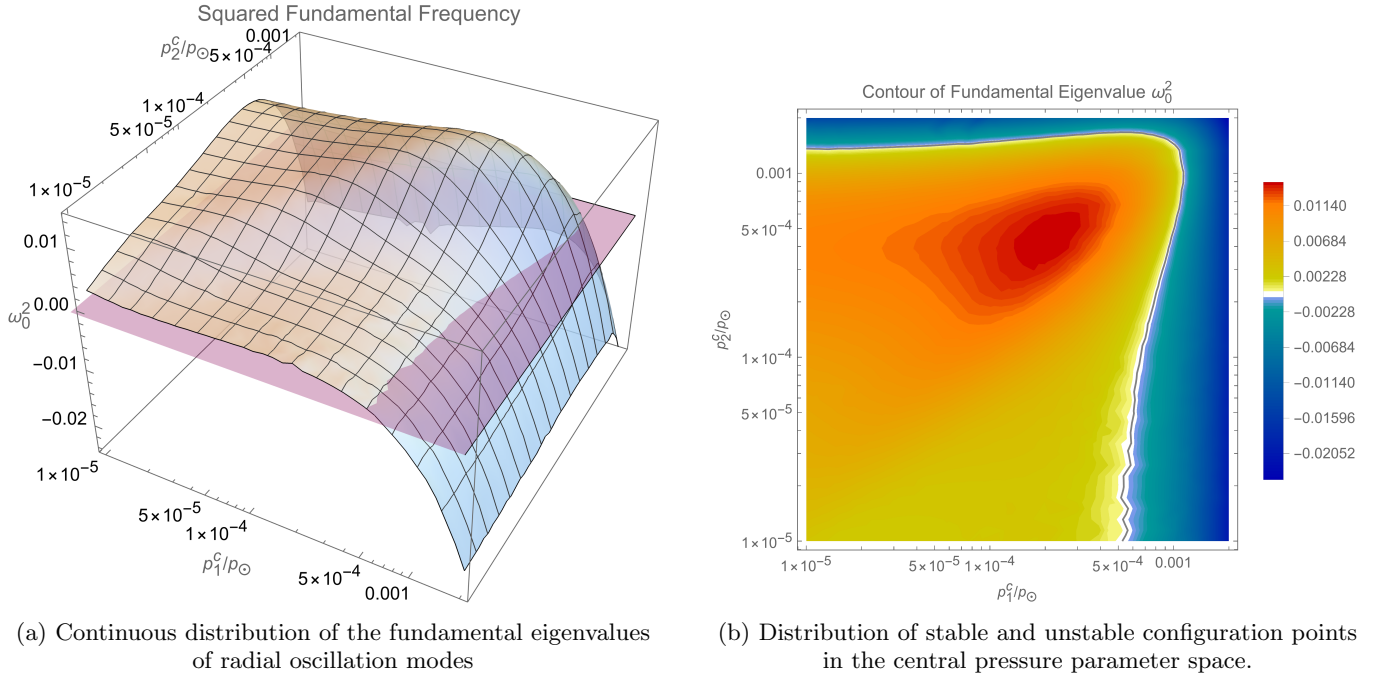


FIG. 4: Radial oscillation analysis results for the mixed star model with EoS of Holographic NM ($\ell^{-7} = 10300$) and Bosonic DM ($B_4 = 0.1$). Left panel (Fig.4a) shows the continuous distribution of eigenvalues. Right panel (Fig.4b) displays the distribution of stable and unstable configuration points in the central pressure parameter space, where the black curve represents configurations where the fundamental radial mode frequency vanishes and its interior indicates the stable region.

EoS: SLy4, Bosonic DM (with $B_4 = 0.1$) and Holographic NM (with $\ell^{-7} = 10300$). The stability distribution and M - R relations satisfy the BTM criteria. These numeri-

cal results serve as comparisons for the situation of mixed components.

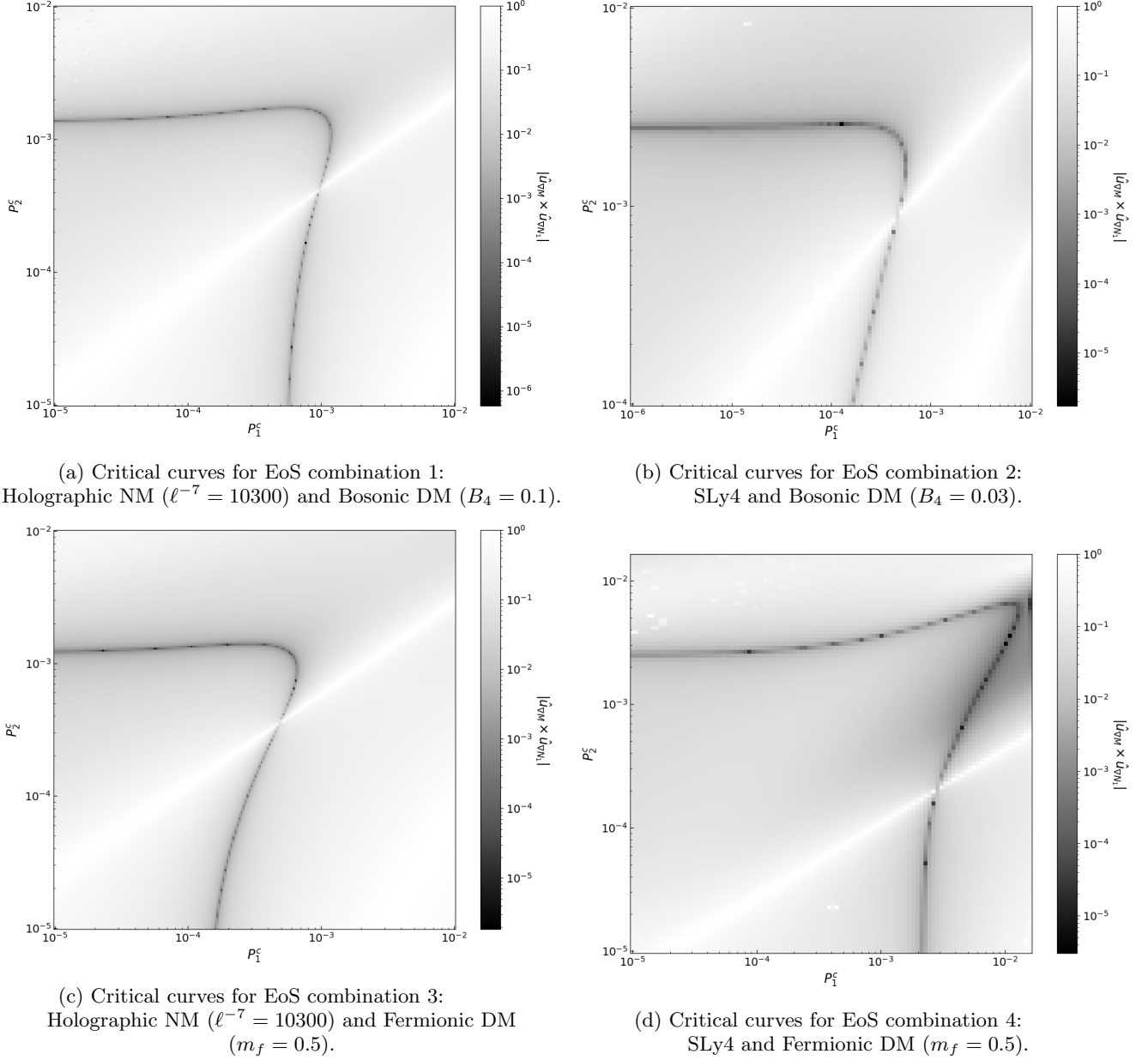


FIG. 5: Critical curves for different EoS combinations. The black curves indicate multiple stability boundaries. The units of both the horizontal and vertical axes are in astrophysical units (p_\odot), representing the magnitudes of central pressure for the two components. The black-and-white heatmap in the background displays the normalized cross product of the gradient directions at each point of the total mass field and the particle number field of the second component; the darker the color, the more the gradient directions of the two fields at that point tend to be parallel. $N_1 \equiv N_{DM}$, represents the DM particle number.

2. Multi-Fluid

The numerical results in Fig.4a provides precise squared frequencies of fundamental radial oscillation using Bosonic DM ($B_4 = 0.1$) and Holographic NM ($\ell^{-7} = 10300$), thus in addition to identifying stable regions, it also reveals the trend of fundamental frequency variation, showing non-monotonic behavior.

To numerically identify the stability boundary statically, we need to precisely identify where the gradients become parallel. Previous work usually relied on connecting the tangent points of several contour lines of mass and particle number [56, 80]. We adopted a more efficient numerical method via computing the magnitude of the normalized cross product between the gradients. Specifically, for any two of the quantities among gravitational

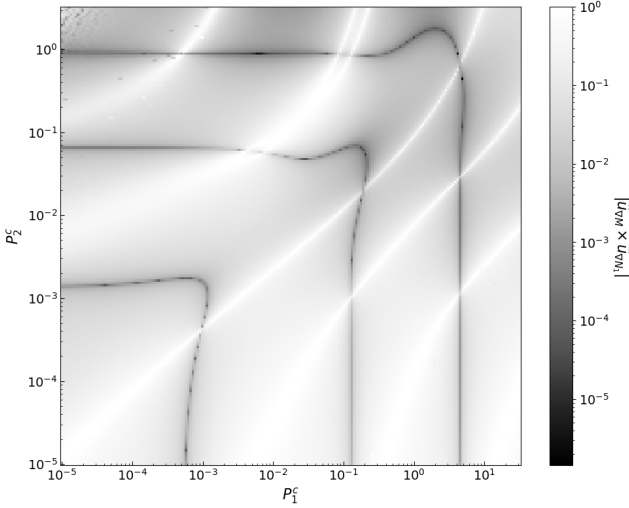


FIG. 6: The critical curves corresponding to the disappearance of higher-order modes. The units of both the horizontal and vertical axes are in astrophysical units (p_\odot). This analysis constitutes an extension of Fig.5a to a larger parameter space, applying the same EoS combination. The dark curves represent zero-mode boundaries ($\omega_n^2 = 0$) for the fundamental mode (innermost curve) as well as the 2nd and 3rd order modes (outer nested curves). The appearance of these outer curves signifies the onset of additional unstable modes in regions of higher central pressures. The white highlight corresponds to the line of maximum gradient angle difference between M and N_{DM} .

mass M and particle number N_I , this cross product is defined as:

$$\mathcal{C}_{M,N_I} = |\hat{u}_{\nabla M} \times \hat{u}_{\nabla N_I}| \equiv \left| \frac{\nabla M}{|\nabla M|} \times \frac{\nabla N_I}{|\nabla N_I|} \right|. \quad (57)$$

Here, $\hat{u}_{\nabla M}$ and $\hat{u}_{\nabla N_I}$ are the normalized gradient direction vectors of the M -field and the N_I -field respectively. The locus where this value becomes numerically zero forms the critical curve. Fig.5 lists critical curve results for different EoS combinations using method introduced in subsection III B. Fig.5a uses Holographic NM with $\ell^{-7} = 10300$ and Bosonic DM with $B_4 = 0.1$. Fig.5b uses SLy4 and Bosonic DM with $B_4 = 0.03$. Fig.5c uses Holographic NM with $\ell^{-7} = 10300$ and Fermionic DM with $m_f = 0.5$. Fig.5d uses SLy4 and Fermionic DM with $m_f = 0.5$. It is clear that Fig.4b and Fig.5a verify the equivalence between the radial oscillation normal mode analysis and critical curve criterion.

Fig.6 extends the analysis of Fig.5a to a larger parameter space, showing critical curves where frequencies higher than the fundamental mode vanish, i.e., boundaries where additional unstable modes appear. Our analytical method involves scanning the parameter space and computing the angular difference between the gradients of two distributions: total mass and particle number.

This allows us to identify points where they are parallel, which are the critical points. Darker regions in the plot indicate smaller angular differences, so the black curves represent our zero-mode boundaries. The white highlight corresponds to the line of maximum gradient angle difference between M and N_1 . Here and later $N_1 \equiv N_{DM}$, representing the DM particle number. Moreover, from the perspective of numerical results, the white lines in Fig.5 and the central white line in Fig.6 coincides exactly with the line where the radii of the two fluid components are equal.

Fig.9a shows the M - R curves for mixed stars with a fixed Bosonic DM central pressure p_1^c and varying Holographic NM ($\ell^{-7} = 10300$) central pressure p_2^c . These relations obtained through single-parameter variations in mixed star models no longer satisfy the BTM criteria. Furthermore, the deviation from the BTM criteria can be quantitatively analyzed, as demonstrated in Fig.9b. This panel plots the relative separation between the central pressure of the last stable point, $p_{\text{last-stable}}$, and that of the maximum mass configuration, $p_{\text{max-mass}}$, as a function of the DM properties, showing the trend of the systematic separation as it varies with the central pressure and properties of DM.

Crucially, the magnitude of this deviation is highly sensitive to the EoS properties of the admixed DM. As shown, different DM models (e.g., Bosonic DM versus Fermionic DM) and variations in their microphysical parameters (such as the interaction strength B_4 or the fermion mass m_f) lead to distinctly different deviation curves. This suggests that the degree to which the BTM criteria is violated is not universal but is instead an indirect probe of the DM's EoS and its gravitational coupling with the NM. Therefore, a precise future measurement of a mixed star's mass, radius, and its stability threshold could, in principle, provide a tool to constrain the nature of DM within the star.

B. Analysis and application of macroscopic quantities

1. M - R Relation

The stable region of equilibrium configurations maps to a continuous topological correspondence region in the M - R - p_I^c space: a two-dimensional surface in three-dimensional space, as shown in Fig.7. The EoS in Fig.7 is Holographic NM ($\ell^{-7} = 10300$) and Bosonic DM ($B_4 = 0.1$), with vertical axis p_1^c in Fig.7a and p_2^c in Fig.7b. R_t is the total radius: $R_t = \max(R_N, R_D)$. Here R_N and R_D represents the radius of NM and DM. Red and blue dots code the configurations where $R_N > R_D$ and $R_N < R_D$. Any slice along the p_I^c axis corresponds to an M - R curve governed by single parameter variation.

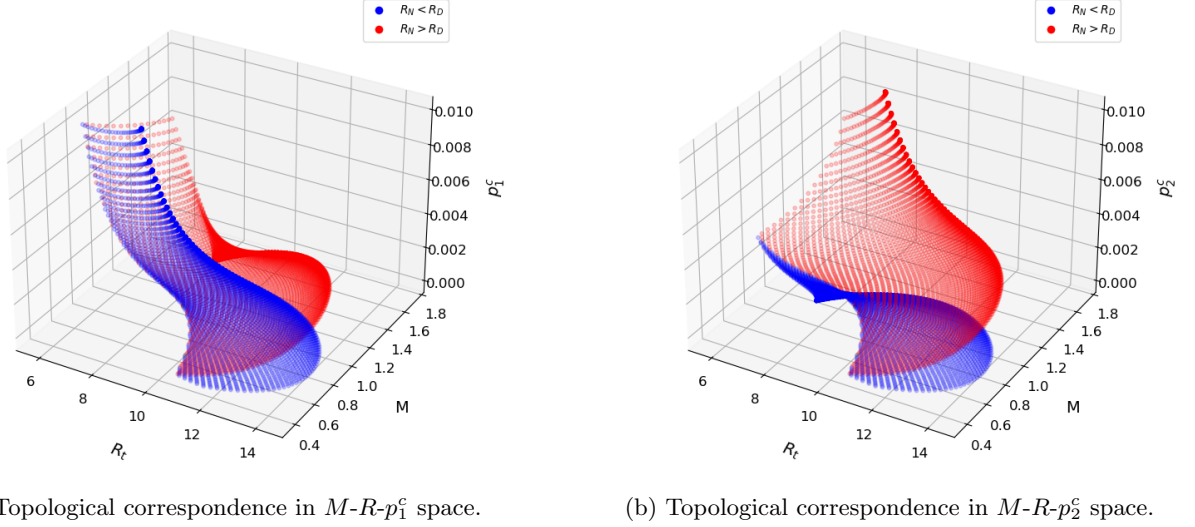


FIG. 7: The two-dimensional stable region from the pressure parameter space is mapped onto a three-dimensional space with axes representing the total mass (in M_\odot unit), the total radius $R_t = \max(R_N, R_D)$ (in km unit), and one of the central pressures (e.g., p_1^c and p_2^c in p_\odot unit). This unfolds the degeneracies of the two-dimensional M - R projection. The red and blue dots distinguishes configurations where the NM radius is larger than the DM radius ($R_N > R_D$, blue) from those where it is smaller ($R_N < R_D$, red). (a) and (b) show the two-dimensional surface of DM and NM pressure for EoS combination in Fig.5a, Holographic NM ($\ell^{-7} = 10300$) and Bosonic DM ($B_4 = 0.1$).

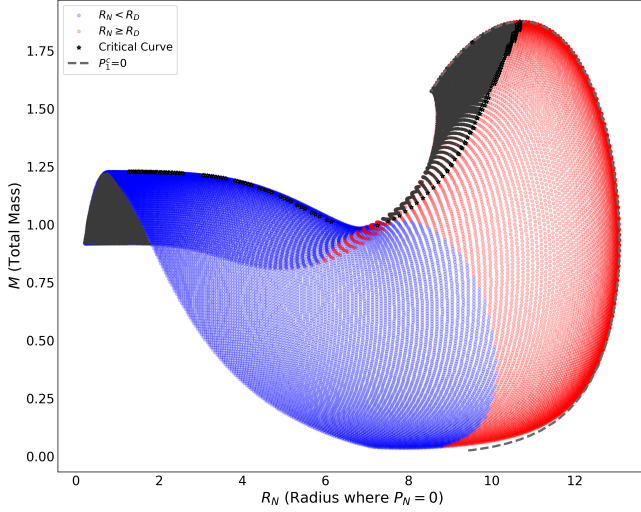
Fig.8 shows the projections of stable configurations onto both the mass-visible radius plane M - R_N and mass-total radius plane M - R_t with EoS combination: Holographic NM ($\ell^{-7} = 10300$) and Bosonic DM ($B_4 = 0.1$). Points within the stability boundary form a “stable group” in the projection plane, serving as a comparison tool for observational data. Overlapping regions of two colors imply the possible existence of “twin configurations” with identical mass and radius but distinct halo compositions. The left boundary line of the “stable group” in Fig.8b coincides with the curve where the radius size relationship between the two fluid components reverses, meaning that for mixed star models with the same mass, the stable configuration that minimizes the total star radius is always the one where the two fluid components have equal radii.

2. Prediction prospects

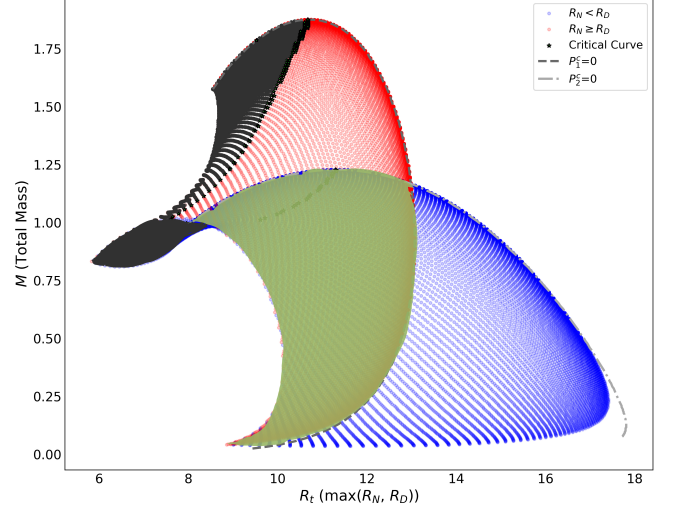
Collecting the latest M - R credible window from observational data of compact stars on the M - R stable groups can impose constraints on DM EoS. Our mixed star model demonstrates the ability to cover a wide range of M - R area by adjusting the EoS parameters. For instance, Fig.8a covers the mass and radius values of data PSR J0437-4715 from the latest NICER observations ($M = 1.418 \pm 0.037 M_\odot$, $R = 11.36^{+0.95}_{-0.63}$ km) [73].

Fig.10 and Table. I show the predicted range of M - R relations and compactness analysis of mixed stars under different EoS parameter selections and different DM

mixing ratios ($ratio \equiv p_{DM}^c/p_{NM}^c$, the central pressure ratio of DM and NM), indicating that by appropriately adjusting the hardness of the EoS and the ratios of admixed DM, the mixed star models have the potential to become predictive for NS and certain gap events, containing ranges of both $3 \sim 5 M_\odot$ and $50 \sim 100 M_\odot$ [34, 90]. In addition, the similar values of compactness M/R for the same EoS combinations but with different parameters and mixing ratios exhibits a slight violation from scaling symmetry for certain kind of single EoS [34, 91]. Moreover, Fig.10b also shows the situations of massive stars with the observable radius of conventional compact stars and accompanied by a large dark halo.

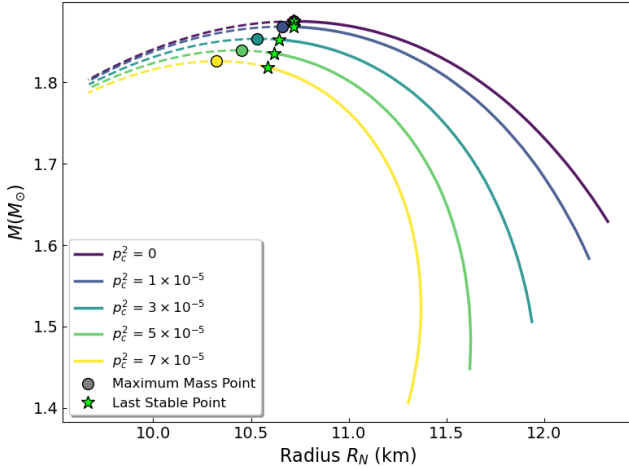


(a) The stable group projected onto the mass versus visible radius plane using Holographic NM and Bosonic DM ($B_4 = 0.1$).

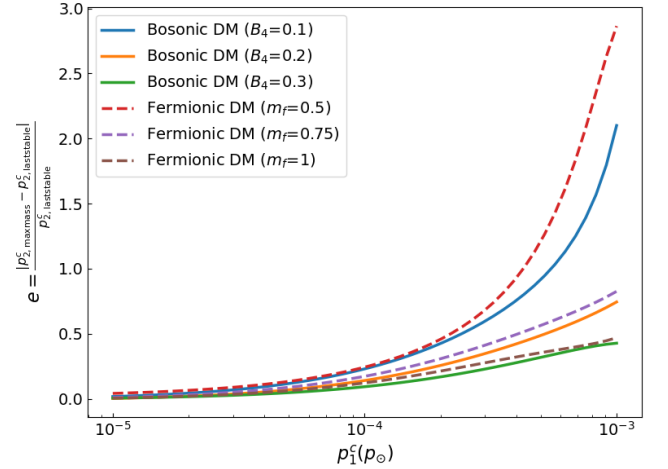


(b) The same stable group projected onto the mass versus maximum radius plane (M - R_t), where $R_t = \max(R_N, R_D)$.

FIG. 8: In both panels, R_N and R_D are the radius(in km unit) where the nuclear and DM pressure vanish, respectively. The colored regions represent dynamically stable configurations, while the grey shaded areas are unstable. The color coding within the stable group distinguishes between Dark Core configurations ($R_N > R_D$, red) and Dark Halo configurations ($R_N < R_D$, blue). The overlapping area between the red and blue regions, highlighted in yellow, indicates the parameter space where **twin stars** [89] can exist: configurations with identical mass and radius but different internal structures (one being a Dark Core, the other a Dark Halo). The dashed line represents the boundary of the stable region (the critical curve).



(a) M - R curves for mixed stars with a fixed Bosonic DM central pressure p_1^c and varying Holographic NM ($\ell^{-7} = 10300$) central pressure p_2^c . The maximum mass point (circle marker) and the last stable configuration point (star marker), determined by the critical curve method, do not coincide.



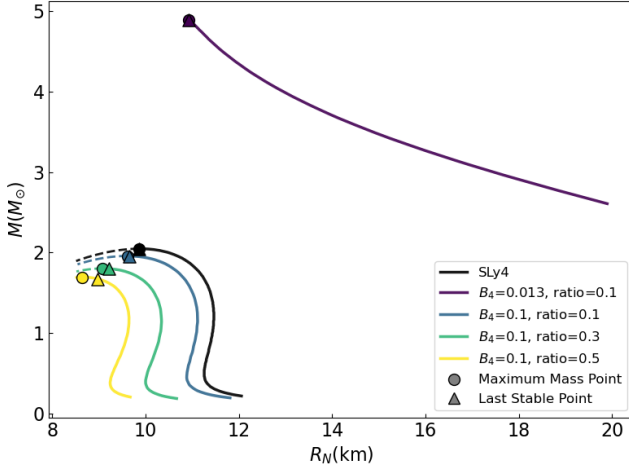
(b) The deviation is described as the relative error between the central pressure of the last stable point and that of the maximum mass point, and it is a function of the DM central pressure p_1^c . This explicitly shows that the turning point of stability deviates from the mass peak, invalidating the simple BTM criteria for these sequences.

FIG. 9: Deviation from the BTM criteria in mixed stars.

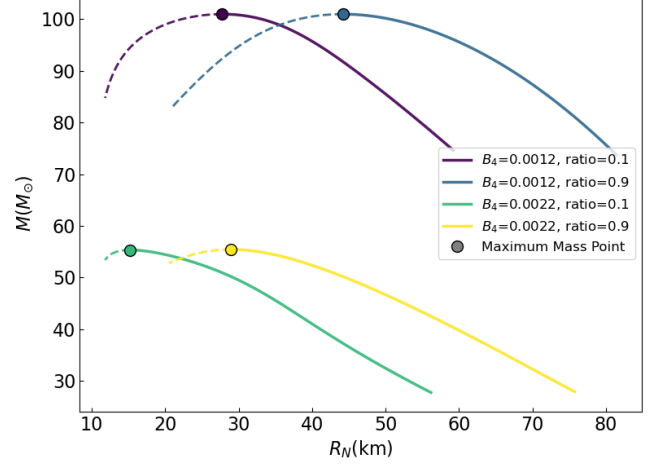
V. CONCLUSION

In this work, we have conducted a comprehensive investigation into the stability properties and macroscopic

characteristics of DM-NM mixed stars within the framework of general relativity.



(a) The M - R relationship with different parameter settings and different mixing ratios ($ratio \equiv p_{DM}^c/p_{NM}^c$) of DM central pressure, where the mass data is within the Oppenheimer limit and near the mass gap, respectively.



(b) Similar settings to the left panel, but with a larger range of total mass.

FIG. 10: Prediction prospects for admixed star models displayed through the M - R relationship, with EoS combination2: Bosonic DM (10) and SLy4.

TABLE I: Maximum mass and corresponding Variables for different EoS parameters and Mixture ratio of DM

Parameter combinations	M_{\max} (M_{\odot})	R_N (km)	R_D (km)	R_t (km)	M/R_N	M/R_D	p_2^c (p_{\odot})
B=0.0012, ratio=0.1	100.98	27.200	870.02	870.02	3.71	0.116	1.0481×10^{-6}
B=0.0022, ratio=0.1	55.340	15.254	495.75	495.75	3.63	0.112	3.5565×10^{-6}
B=0.0012, ratio=0.9	100.97	44.668	878.50	878.50	2.26	0.115	1.0000×10^{-7}
B=0.0022, ratio=0.9	55.434	29.046	494.51	494.51	1.91	0.112	3.3932×10^{-7}

We have established a formal equivalence between the critical curve method and the traditional oscillation approach, based on both conservation laws and the variational principle.

Our numerical calculations, employing four typical EoS combinations: SLy4, Holographic NM, Fermionic DM and Bosonic DM, determine the stability regions of mixed stars and validate the equivalence between the two methods numerically, while revealing complex stability distributions that fundamentally differ from single-fluid stars and hybrid stars. Unlike pure NS that obey the classical BTM criteria, mixed stars stable configurations form continuous two-dimensional surfaces in the three-dimensional parameter space of (one of the) central pressure, mass, and radius. The projection of these stable configurations onto the M - R plane reveals “stable group” that delineate natural regions where mixed stars should be observationally found. These groups exhibit several noteworthy features, including the existence of twin configurations with identical M - R measurements but different internal compositions, and the characteristic property that the most compact stable configurations correspond to equal radii of the two fluid components. moreover, our mixed star model, by adjusting the EoS

hardness and DM ratio, can fit regular NS events and explain certain mass-gap events. It also has the potential to predict massive configurations featuring a compact star radius core alongside a large DM halo.

Looking forward, our theoretical framework can be extended to incorporate more sophisticated DM models, for example self-interacting fermionic DM and axion-like particles. The methodology also provides a foundation for investigating rotating mixed stars, magnetic field effects, and dynamical formation scenarios. As observational capabilities continue to advance, the stable groups and characteristic M - R relations identified through our analysis may serve as references for identifying potential mixed star candidates and constraining the properties of DM through astrophysical observations.

ACKNOWLEDGMENTS

The authors would like to thank Feng-Li Lin, Dong Lai, Qiyuan Pan, Shao-Feng Ge, Zhoujian Cao, Nobutoshi Yasutake, Chian-Shu Chen, Alessandro Parisi, Chen Zhang, Zihao Zhang, Hao Feng and Jing-Yi Wu for helpful discussions. KZ (Hong Zhang) is supported by a classified fund from Shanghai city.

Appendix A: Detailed Proof of the variational extremum theorem

We aim to prove Theorem III.2 that for an isentropic two-fluid system. The star configuration satisfies the equilibrium equations if and only if the quantity M is defined by:

$$M \equiv \sum_{I=1,2} \int_0^{R_I} 4\pi r^2 \varepsilon_I(r) dr \quad (\text{A1})$$

is extremal under all variations of $\varepsilon_I(r)$ that keep the quantities

$$N_I \equiv \int_0^{R_I} 4\pi r^2 n_I(r) \left[1 - \frac{2m_t(r)}{r} \right]^{-\frac{1}{2}} dr \quad (\text{A2})$$

constant for $I = 1, 2$. This is equivalent to the existence of Lagrange multipliers λ_1 and λ_2 such that $\delta H = \delta M - \lambda_1 \delta N_1 - \lambda_2 \delta N_2$ is zero for all variations.

For given variations $\delta \varepsilon_I(r)$, we have:

$$\begin{aligned} \delta H [\{\delta \varepsilon_I(r)\}] &= \delta M [\{\delta \varepsilon_I(r)\}] - \lambda_1 \delta N_1 [\{\delta \varepsilon_I(r)\}] \\ &\quad - \lambda_2 \delta N_2 [\{\delta \varepsilon_I(r)\}]. \end{aligned} \quad (\text{A3})$$

Now expand each term as (since all the integrand vanishes above $R_I + \delta R_I$, we write the upper limit of integration as positive infinity)

$$\begin{aligned} \delta M &= 4\pi \sum_{I=1,2} \int_0^{R_I+\infty} r^2 \delta \varepsilon_I(r) dr, \\ \delta N_I &= 4\pi \int_0^\infty r^2 \left(1 - \frac{2m_t(r)}{r} \right)^{-1/2} \delta n_I(r) dr \\ &\quad + 4\pi \int_0^\infty r \left(1 - \frac{2m_t(r)}{r} \right)^{-3/2} \\ &\quad \times n_I(r) \delta m_t(r) dr, \end{aligned} \quad (\text{A4})$$

where $m_t(r) = m_1(r) + m_2(r)$. Thus:

$$\begin{aligned} \delta H &= 4\pi \sum_{I=1,2} \int_0^\infty r^2 \delta \varepsilon_I(r) dr - 4\pi \sum_{I=1,2} \lambda_I \\ &\quad \times \left[\int_0^\infty r^2 \left(1 - \frac{2m_t}{r} \right)^{-\frac{1}{2}} \delta n_I(r) dr \right. \\ &\quad \left. + \sum_{J=1,2} \int_0^\infty r \left(1 - \frac{2m_t}{r} \right)^{-\frac{3}{2}} n_I(r) \delta m_J(r) dr \right]. \end{aligned} \quad (\text{A5})$$

Using the isentropic conditions:

$$\delta n_I(r) = \frac{n_I(r)}{p_I(r) + \varepsilon_I(r)} \delta \varepsilon_I(r) \quad (\text{A6})$$

and the mass variation:

$$\delta m_I(r) = 4\pi \int_0^r r'^2 \delta \varepsilon_I(r') dr', \quad (\text{A7})$$

We do substitution by steps. First, substitute δn_I :

$$\begin{aligned} \delta H &= 4\pi \sum_{I=1,2} \int_0^\infty r^2 \delta \varepsilon_I(r) dr - 4\pi \sum_{I=1,2} [\lambda_I \\ &\quad \times \int_0^\infty r^2 \left(1 - \frac{2m_t}{r} \right)^{-\frac{1}{2}} \frac{n_I(r)}{p_I(r) + \varepsilon_I(r)} \delta \varepsilon_I(r) dr] \\ &\quad - 4\pi \sum_{I=1,2} \lambda_I \sum_{J=1,2} \int_0^\infty \left[r \left(1 - \frac{2m_t}{r} \right)^{-\frac{3}{2}} \right. \\ &\quad \left. n_I(r) \delta m_J(r) dr \right]. \end{aligned} \quad (\text{A8})$$

Now substitute $\delta m_J(r)$ into the last term:

$$\begin{aligned} &- 4\pi \sum_{I=1,2} \lambda_I \sum_{J=1,2} \int_0^\infty r \left(1 - \frac{2m_t}{r} \right)^{-\frac{3}{2}} \\ &\quad n_I(r) \left[4\pi \int_0^r r'^2 \delta \varepsilon_J(r') dr' \right] dr \end{aligned} \quad (\text{A9})$$

Defining

$$D(r) = \sum_{K=1,2} \lambda_K \int_r^\infty dr' r' \left(1 - \frac{2m_t(r')}{r'} \right)^{-\frac{3}{2}} n_K(r') \quad (\text{A10})$$

and exchanging the order of integration in the double integral, the last term becomes:

$$-16\pi^2 \sum_{J=1,2} \int_0^\infty dr r^2 \delta \varepsilon_J(r) D(r) \quad (\text{A11})$$

Now combine all terms in δH :

$$\begin{aligned}
\delta H &= 4\pi \sum_{I=1,2} \int_0^\infty r^2 \delta \varepsilon_I(r) dr - 4\pi \sum_{I=1,2} \lambda_I \int_0^\infty r^2 \left(1 - \frac{2m_t(r)}{r}\right)^{-\frac{1}{2}} \frac{n_I(r)}{p_I(r) + \varepsilon_I(r)} \delta \varepsilon_I(r) dr \\
&\quad - 16\pi^2 \sum_{J=1,2} \int_0^\infty dr r^2 \delta \varepsilon_J(r) D(r) \\
&= 4\pi \sum_{I=1,2} \int_0^\infty r^2 \delta \varepsilon_I(r) \left[1 - \lambda_I \left(1 - \frac{2m_t(r)}{r}\right)^{-\frac{1}{2}} \frac{n_I(r)}{p_I(r) + \varepsilon_I(r)} - 4\pi D(r) \right] dr \\
&= 4\pi \sum_{I=1,2} \int_0^\infty r^2 \delta \varepsilon_I(r) \left[1 - \lambda_I \left(1 - \frac{2m_t(r)}{r}\right)^{-\frac{1}{2}} \frac{n_I(r)}{p_I(r) + \varepsilon_I(r)} - 4\pi \sum_{J=1,2} \lambda_J \int_r^\infty r' \left(1 - \frac{2m_t(r')}{r'}\right)^{-\frac{3}{2}} n_J(r') dr' \right] dr.
\end{aligned} \tag{A12}$$

For δH to be zero for all variations $[\{\delta \varepsilon_I(r)\}]$, the integrand must vanish for each fluid component I :

$$\begin{aligned}
1 - \lambda_I A(r)^{-1/2} \frac{n_I(r)}{p_I(r) + \varepsilon_I(r)} \\
- 4\pi \sum_{J=1,2} \lambda_J \int_r^\infty r' A(r')^{-3/2} n_J(r') dr' = 0,
\end{aligned} \tag{A13}$$

where $A(r) = 1 - \frac{2m_t(r)}{r}$. This is the extremization condition for the two-fluid system.

Define:

$$F(r) = 4\pi \sum_{J=1,2} \lambda_J \int_r^\infty r' A(r')^{-3/2} n_J(r') dr'. \tag{A14}$$

Then the condition becomes:

$$\lambda_I A(r)^{-1/2} \frac{n_I(r)}{p_I(r) + \varepsilon_I(r)} + F(r) = 1 \quad \text{for } I = 1, 2. \tag{A15}$$

From these two equations, we obtain a key constraint that reflects the effect of Lagrange multipliers in this two-fluid system:

$$\lambda_1 A(r)^{-1/2} \frac{n_1(r)}{p_1(r) + \varepsilon_1(r)} = \lambda_2 A(r)^{-1/2} \frac{n_2(r)}{p_2(r) + \varepsilon_2(r)}, \tag{A16}$$

which implies:

$$\frac{\lambda_1 n_1}{p_1 + \varepsilon_1} = \frac{\lambda_2 n_2}{p_2 + \varepsilon_2}. \tag{A17}$$

This reflects that the chemical potential between the two fluids satisfies a proportional relationship, which is somewhat different from the case of a single fluid.

Define a common function:

$$\Gamma(r) = \lambda_I \frac{n_I(r)}{p_I(r) + \varepsilon_I(r)}, \quad \text{for } I = 1, 2. \tag{A18}$$

Differentiate the condition with respect to r :

$$\begin{aligned}
\frac{d}{dr} \left[\lambda_I A(r)^{-1/2} \frac{n_I(r)}{p_I(r) + \varepsilon_I(r)} \right] + F'(r) &= 0, \\
\text{for } I = 1, 2.
\end{aligned} \tag{A19}$$

where:

$$F'(r) = -4\pi \sum_{J=1,2} \lambda_J r A(r)^{-3/2} n_J. \tag{A20}$$

Take the derivative in (A19) and substitute the isentropic condition $n'_I = \frac{n_I \varepsilon'_I}{p_I + \varepsilon_I}$:

$$\begin{aligned}
\lambda_I \left[-n_I A^{-1/2} \frac{p'_I}{(p_I + \varepsilon_I)^2} \right. \\
\left. - \frac{1}{2} n_I A^{-3/2} \frac{A'}{p_I + \varepsilon_I} \right] - 4\pi \sum_{J=1,2} \lambda_J r A^{-3/2} n_J = 0,
\end{aligned} \tag{A21}$$

for $I = 1, 2$.

Multiply by $A^{3/2}$ and $(p_I + \varepsilon_I)^2$, then rearrange to solve for p'_I :

$$p'_I = -\frac{1}{2} \frac{A'}{A} (p_I + \varepsilon_I) - 4\pi \frac{\sum_{J=1,2} \lambda_J r n_J}{\lambda_I n_I A} (p_I + \varepsilon_I)^2. \tag{A22}$$

From the constraint definition $\Gamma(r) = \lambda_I \frac{n_I}{p_I + \varepsilon_I}$, we have:

$$\lambda_I n_I = \Gamma(r) (p_I + \varepsilon_I), \tag{A23}$$

$$\sum_{J=1,2} \lambda_J n_J = \Gamma(r) (p_1 + \varepsilon_1 + p_2 + \varepsilon_2) = \Gamma(r) (p_t + \varepsilon_t), \tag{A24}$$

Thus:

$$\frac{\sum_{J=1,2} \lambda_J n_J}{\lambda_I n_I} = \frac{p_t + \varepsilon_t}{p_I + \varepsilon_I}. \tag{A25}$$

Substitute back to (A22):

$$\begin{aligned}
p'_I &= -\frac{1}{2} \frac{A'}{A} (p_I + \varepsilon_I) - 4\pi r \frac{p_t + \varepsilon_t}{A} (p_I + \varepsilon_I) \\
&= -(p_I + \varepsilon_I) \left(\frac{1}{2} \frac{A'}{A} + 4\pi r \frac{p_t + \varepsilon_t}{A} \right).
\end{aligned} \tag{A26}$$

Now compute A' : using $m'_t = 4\pi r^2 \varepsilon_t$ we obtain

$$A' = 2 \left(\frac{m_t}{r^2} - 4\pi r \varepsilon_t \right). \quad (\text{A27})$$

Substitute into the expression for p'_I :

$$\begin{aligned} p'_I &= -(p_I + \varepsilon_I) \frac{1}{A} \left(\frac{1}{2} A' + 4\pi r (p_t + \varepsilon_t) \right) \\ &= -(p_I + \varepsilon_I) \frac{1}{A} \left(\frac{m_t}{r^2} + 4\pi r p_t \right) \\ &= -(p_I + \varepsilon_I) \frac{m_t + 4\pi r^3 p_t}{r(r - 2m_t)}. \end{aligned} \quad (\text{A28})$$

This is exactly the two-fluid equilibrium equation:

$$\frac{dp_I}{dr} = -(\varepsilon_I(r) + p_I(r)) \frac{m_t(r) + 4\pi r^3 p_t(r)}{r(r - 2m_t(r))}, \quad (\text{A29})$$

for $I = 1, 2$.

-
- [1] B. P. Abbott, R. Abbott, and e. a. Abbott (LIGO Scientific Collaboration and Virgo Collaboration), Gw170817: Observation of gravitational waves from a binary neutron star inspiral, *Phys. Rev. Lett.* **119**, 161101 (2017).
 - [2] S. Chandrasekhar, The Dynamical Instability of Gaseous Masses Approaching the Schwarzschild Limit in General Relativity, *Astrophys. J.* **140**, 417 (1964).
 - [3] J. M. Bardeen, K. S. Thorne, and D. W. Meltzer, A catalog of methods for studying the normal modes of radial pulsation of general-relativistic stellar models, *The Astrophysical Journal* **145**, 505 (1966).
 - [4] H. MISHRA, S. MISRA, P. PANDA, and B. PARIDA, Neutron matter – quark matter phase transition and quark star, *International Journal of Modern Physics E* **02**, 547–563 (1993).
 - [5] S. K. Ghosh, S. C. Phatak, and P. K. Sahu, Hybrid stars and quark hadron phase transition in chiral colour dielectric model, *Zeitschrift für Physik A Hadrons and Nuclei* **352**, 457–466 (1995).
 - [6] S. KHADKIKAR, A. MISHRA, and H. MISHRA, Confinement, quark matter equation of state and hybrid stars, *Modern Physics Letters A* **10**, 2651–2663 (1995).
 - [7] F. Di Clemente, M. Mannarelli, and F. Tonelli, Reliable description of the radial oscillations of compact stars, *Physical Review D* **101**, 10.1103/physrevd.101.103003 (2020).
 - [8] A. Henriques, A. R. Liddle, and R. Moorhouse, Stability of boson-fermion stars, *Physics Letters B* **251**, 511 (1990).
 - [9] N. Zhang, B.-A. Li, J. Zhang, W. Shen, and H. Zhang, Illuminating dark matter admixed in neutron stars with simultaneous mass–radius constraints, *Symmetry* **17**, 1669 (2025).
 - [10] G. Panotopoulos, How compact stars challenge our view about dark matter (2019), arXiv:1910.02279 [gr-qc].
 - [11] Z. Rezaei, Double dark matter admixed neutron star, *International Journal of Modern Physics D* **27**, 1950002 (2018).
 - [12] X. D. Wang, B. Qi, G. L. Yang, N. B. Zhang, and S. Y. Wang, Possible maximum mass of dark matter existing in compact stars based on the self-interacting fermionic model, *International Journal of Modern Physics D* **28**, 1950148 (2019).
 - [13] P. Mukhopadhyay and J. Schaffner-Bielich, Quark stars admixed with dark matter, *Physical Review D* **93**, 10.1103/physrevd.93.083009 (2016).
 - [14] Q.-F. Xiang, W.-Z. Jiang, D.-R. Zhang, and R.-Y. Yang, Effects of fermionic dark matter on properties of neutron stars, *Physical Review C* **89**, 10.1103/physrevc.89.025803 (2014).
 - [15] S.-C. Leung, M.-C. Chu, and L.-M. Lin, Dark-matter admixed neutron stars, *Physical Review D* **84**, 10.1103/physrevd.84.107301 (2011).
 - [16] S.-C. Leung, M.-C. Chu, and L.-M. Lin, Equilibrium structure and radial oscillations of dark matter admixed neutron stars, *Physical Review D* **85**, 10.1103/physrevd.85.103528 (2012).
 - [17] K. Zhang, G.-Z. Huang, J.-S. Tsao, and F.-L. Lin, Gw170817 and gw190425 as hybrid stars of dark and nuclear matter, *The European Physical Journal C* **82**, 1 (2022).
 - [18] B. Kain, Radial oscillations and stability of multiple-fluid compact stars, *Phys. Rev. D* **102**, 023001 (2020), arXiv:2007.04311 [gr-qc].
 - [19] B. Kain, Dark matter admixed neutron stars, *Phys. Rev. D* **103**, 043009 (2021), arXiv:2102.08257 [gr-qc].
 - [20] T.-S. Chen, X.-D. Zhou, and K. Zhang, Equivalence of stability criteria for multi-fluid stars, to appear (2025).
 - [21] R. C. Tolman, Static solutions of einstein’s field equations for spheres of fluid, *Phys. Rev.* **55**, 364 (1939).
 - [22] J. R. Oppenheimer and G. M. Volkoff, On massive neutron cores, *Physical Review* **55**, 374 (1939).
 - [23] G. Panotopoulos and I. Lopes, Dark matter effect on realistic equation of state in neutron stars, *Physical Review D* **96**, 083004 (2017).
 - [24] S.-C. Leung, M.-C. Chu, and L.-M. Lin, Dark-matter admixed neutron stars, *Physical Review D—Particles, Fields, Gravitation, and Cosmology* **84**, 107301 (2011).
 - [25] E. Kolb, *The early universe* (CRC press, 2018).
 - [26] F. D. Steffen, Dark-matter candidates: Axions, neutrali-

- nos, gravitinos, and axinos, *The European Physical Journal C* **59**, 557 (2009).
- [27] T. Güver, A. E. Erkoca, M. H. Reno, and I. Sarcevic, On the capture of dark matter by neutron stars, *Journal of Cosmology and Astroparticle Physics* **2014** (05), 013.
- [28] H. Davoudiasl, Gravitationally induced dark matter asymmetry and dark nucleon decay, *Phys. Rev. D* **88**, 095004 (2013).
- [29] A. R. Zentner and A. P. Hearin, Asymmetric dark matter may alter the evolution of very low-mass stars and brown dwarfs, *Phys. Rev. D* **84**, 101302 (2011).
- [30] S. Tulin and H.-B. Yu, Dark matter self-interactions and small scale structure, *Physics Reports* **730**, 1–57 (2018).
- [31] L. G. van den Aarssen, T. Bringmann, and C. Pfrommer, Is dark matter with long-range interactions a solution to all small-scale problems of Λ cold dark matter cosmology?, *Physical Review Letters* **109**, 10.1103/physrevlett.109.231301 (2012).
- [32] S. Tulin, H.-B. Yu, and K. M. Zurek, Resonant dark forces and small-scale structure, *Phys. Rev. Lett.* **110**, 111301 (2013).
- [33] J. L. Feng, M. Kaplinghat, and H.-B. Yu, Halo-shape and relic-density exclusions of sommerfeld-enhanced dark matter explanations of cosmic ray excesses, *Physical Review Letters* **104**, 10.1103/physrevlett.104.151301 (2010).
- [34] K. Zhang, L.-W. Luo, J.-S. Tsao, C.-S. Chen, and F.-L. Lin, Dark stars and gravitational waves: Topical review, *Results in Physics*, 106967 (2023).
- [35] E. Aprile, K. Arisaka, F. Arneodo, *et al.* (XENON100 Collaboration), First dark matter results from the xenon100 experiment, *Phys. Rev. Lett.* **105**, 131302 (2010).
- [36] Z. Ahmed, D. S. Akerib, S. Arrenberg, *et al.* (CDMS Collaboration), Results from a low-energy analysis of the cdms ii germanium data, *Phys. Rev. Lett.* **106**, 131302 (2011).
- [37] C. E. Aalseth, P. Barbeau, N. Bowden, B. Cabrera-Palmer, J. Colaresi, J. Collar, S. Dazeley, P. De Lurgio, J. E. Fast, N. Fields, *et al.*, Results from a search for light-mass dark matter with a p-type point contact germanium detector, *Physical Review Letters* **106**, 131301 (2011).
- [38] R. Bernabei, P. Belli, F. Cappella, R. Cerulli, C. Dai, A. d'Angelo, H. He, A. Incicchitti, H. Kuang, J. Ma, *et al.*, First results from dama/libra and the combined results with dama/nai, *The European Physical Journal C* **56**, 333 (2008).
- [39] S.-C. Leung, M.-C. Chu, and L.-M. Lin, Dark-matter admixed neutron stars, *Phys. Rev. D* **84**, 107301 (2011).
- [40] I. Goldman and S. Nussinov, Weakly interacting massive particles and neutron stars, *Phys. Rev. D* **40**, 3221 (1989).
- [41] C. Kouvaris, Wimp annihilation and cooling of neutron stars, *Phys. Rev. D* **77**, 023006 (2008).
- [42] G. Bertone and M. Fairbairn, Compact stars as dark matter probes, *Phys. Rev. D* **77**, 043515 (2008).
- [43] A. de Lavallaz and M. Fairbairn, Neutron stars as dark matter probes, *Phys. Rev. D* **81**, 123521 (2010).
- [44] C. Kouvaris and P. Tinyakov, Can neutron stars constrain dark matter?, *Phys. Rev. D* **82**, 063531 (2010).
- [45] R. Brito, V. Cardoso, and H. Okawa, Accretion of dark matter by stars, *Phys. Rev. Lett.* **115**, 111301 (2015).
- [46] M. Cerneno, M. Á. Pérez-García, and J. Silk, Fermionic light dark matter particles and the new physics of neutron stars, *Publications of the Astronomical Society of Australia* **34**, e043 (2017).
- [47] M. I. Gresham and K. M. Zurek, Asymmetric dark stars and neutron star stability, *Physical Review D* **99**, 083008 (2019).
- [48] J. Ellis, G. Hütsi, K. Kannike, L. Marzola, M. Raidal, and V. Vaskonen, Dark matter effects on neutron star properties, *Phys. Rev. D* **97**, 123007 (2018).
- [49] M. Deliyergiyev, A. Del Popolo, L. Tolos, M. Le Delliou, X. Lee, and F. Burgio, Dark compact objects: An extensive overview, *Phys. Rev. D* **99**, 063015 (2019).
- [50] A. E. Nelson, S. Reddy, and D. Zhou, Dark halos around neutron stars and gravitational waves, *Journal of Cosmology and Astroparticle Physics* **2019** (07), 012.
- [51] J. Bramante and N. Raj, Dark matter in compact stars (2025), arXiv:2307.14435 [hep-ph].
- [52] M. Alford, M. Braby, M. Paris, and S. Reddy, Hybrid stars that masquerade as neutron stars, *The Astrophysical Journal* **629**, 969 (2005).
- [53] A. Issifu, A. Konstantinou, P. Thakur, and T. Frederico, Rotating proto-neutron stars admixed with mirror dark matter: A two fluid approach (2025), arXiv:2507.20823 [astro-ph.HE].
- [54] K. Zhang and F.-L. Lin, Constraint on hybrid stars with gravitational wave events, *Universe* **6**, 231 (2020).
- [55] S. L. Pitz and J. Schaffner-Bielich, Generating ultra-compact neutron stars with bosonic dark matter (2024), arXiv:2408.13157 [astro-ph.HE].
- [56] A. Kumar and H. Sotani, Stability analysis of two-fluid neutron stars featuring twin star and ultradense configurations (2025), arXiv:2509.03862 [astro-ph.HE].
- [57] O. Ivanytskyi, V. Sagun, and I. Lopes, Neutron stars: New constraints on asymmetric dark matter, *Physical Review D* **102**, 10.1103/physrevd.102.063028 (2020).
- [58] M. I. Gresham and K. M. Zurek, Asymmetric dark stars and neutron star stability, *Physical Review D* **99**, 10.1103/physrevd.99.083008 (2019).
- [59] J. M. Bardeen, K. S. Thorne, and D. W. Meltzer, A Catalogue of Methods for Studying the Normal Modes of Radial Pulsation of General-Relativistic Stellar Models, *Astrophys. J.* **145**, 505 (1966).
- [60] M. Shahrbafe, D. R. Karkevandi, A. Ayriyan, and S. Typel, Observational probes of the neutron star equation of state with hyperons, bosonic dark matter, and quark matter, arXiv preprint arXiv:2402.18686 (2024).
- [61] M. Shahrbafe, P. Thakur, and D. R. Karkevandi, Probing strange dark matter through f -mode oscillations of neutron stars with hyperons and quark matter (2025), arXiv:2510.08115 [nucl-th].
- [62] S. Mukhopadhyay, D. Atta, K. Imam, D. N. Basu, and C. Samanta, Compact bifluid hybrid stars: hadronic matter mixed with self-interacting fermionic asymmetric dark matter, *The European Physical Journal C* **77**, 10.1140/epjc/s10052-017-5006-3 (2017).
- [63] V. R. Pandharipande, C. J. Pethick, and D. G. Ravenhall, Equation of state and neutron star models, *Nuclear Physics A* **A498**, 313c (1989), proceedings of the International Nuclear Physics Conference, Harrogate, UK.
- [64] A. Akmal, V. Pandharipande, and D. Ravenhall, Equation of state of nucleon matter and neutron star structure, *Physical Review C* **58**, 1804 (1998).
- [65] R. B. Wiringa, V. Fiks, and A. Fabrocini, Equation of

- state for dense nucleon matter, *Physical Review C* **38**, 1010 (1988).
- [66] H. M  ther, M. Prakash, and T. Ainsworth, The nuclear symmetry energy in relativistic brueckner-hartree-fock calculations, *Physics Letters B* **199**, 469 (1987).
 - [67] H. Mueller and B. D. Serot, Relativistic mean-field theory and the high-density nuclear equation of state, *Nuclear Physics A* **606**, 508 (1996).
 - [68] B. D. Lackey, M. Nayyar, and B. J. Owen, Observational constraints on hyperons in neutron stars, *Phys. Rev. D* **73**, 024021 (2006).
 - [69] S. Goriely, N. Chamel, and J. Pearson, Skyrme-hartree-fock-bogoliubov nuclear mass formulas: Crossing the 0.6 mev accuracy threshold with microscopically deduced pairing, *Physical review letters* **102**, 152503 (2009).
 - [70] E. Chabanat, P. Bonche, P. Haensel, J. Meyer, and R. Schaeffer, A skyrme parametrization from subnuclear to neutron star densities part ii. nuclei far from stabilities, *Nuclear Physics A* **635**, 231 (1998).
 - [71] E. Chabanat, P. Bonche, P. Haensel, J. Meyer, and R. Schaeffer, A skyrme parametrization from subnuclear to neutron star densities, *Nuclear Physics A* **627**, 710 (1997).
 - [72] F. Douchin and P. Haensel, A unified equation of state of dense matter and neutron star structure, *Astronomy & Astrophysics* **380**, 151 (2001).
 - [73] D. Choudhury, T. Salmi, S. Vinciguerra, T. E. Riley, Y. Kini, A. L. Watts, B. Dorsman, S. Bogdanov, S. Guillot, P. S. Ray, D. J. Reardon, R. A. Remillard, A. V. Bilous, D. Huppenkothen, J. M. Lattimer, N. Rutherford, Z. Arzumanyan, K. C. Gendreau, S. M. Morsink, and W. C. G. Ho, A nicer view of the nearest and brightest millisecond pulsar: Psr j0437–4715, *The Astrophysical Journal Letters* **971**, L20 (2024).
 - [74] W. Li, J.-Y. Wu, and K. Zhang, Deriving neutron star equation of state from ads/qcd, *Results in Physics* **64**, 107893 (2024).
 - [75] T. Sakai and S. Sugimoto, Low energy hadron physics in holographic qcd, *Progress of Theoretical Physics* **113**, 843–882 (2005).
 - [76] E. Witten, Anti-de sitter space, thermal phase transition, and confinement in gauge theories (1998), arXiv:hep-th/9803131 [hep-th].
 - [77] S. L. Shapiro and S. A. Teukolsky, *Black Holes, White Dwarfs and Neutron Stars: The Physics of Compact Objects* (John Wiley & Sons, New York, 1983).
 - [78] N. K. Glendenning, *Compact Stars: Nuclear Physics, Particle Physics, and General Relativity*, 2nd ed. (Springer, New York, 2000).
 - [79] M. Colpi, S. L. Shapiro, and I. Wasserman, Boson stars: Gravitational equilibria of self-interacting scalar fields, *Physical review letters* **57**, 2485 (1986).
 - [80] S. Valdez-Alvarado, C. Palenzuela, D. Alic, and L. A. Ure  a L  pez, Dynamical evolution of fermion-boson stars, *Phys. Rev. D* **87**, 084040 (2013).
 - [81] M. G. Alford, S. P. Harris, and P. S. Sachdeva, On the Stability of Strange Dwarf Hybrid Stars, *Astrophys. J.* **847**, 109 (2017), arXiv:1707.08631 [nucl-th].
 - [82] D. A. Caballero, J. Ripley, and N. Yunes, Radial mode stability of two-fluid neutron stars, *Physical Review D* **110**, 10.1103/physrevd.110.103038 (2024).
 - [83] D. A. Caballero, J. Ripley, and N. Yunes, Radial mode stability of two-fluid neutron stars, *Phys. Rev. D* **110**, 103038 (2024).
 - [84] J. L. Friedman and N. Stergioulas, *Rotating Relativistic Stars*, Cambridge Monographs on Mathematical Physics (Cambridge University Press, 2013).
 - [85] M. Had  i   and Z. Lin, Turning point principle for relativistic stars, *Communications in Mathematical Physics* **387**, 729 (2021).
 - [86] S. Weinberg, *Gravitation and cosmology: principles and applications of the general theory of relativity* (John Wiley & Sons, 2013).
 - [87] J. L. Friedman, *Lagrangian Perturbation Theory of Non-relativistic Fluids*, (1978).
 - [88] D. Kong, Y. Tian, and H. Zhang, Dynamic and thermodynamic stability of superconducting-superfluid stars (2025), arXiv:2511.03259 [gr-qc].
 - [89] M. Hippert, E. Dillingham, H. Tan, D. Curtin, J. Noronha-Hostler, and N. Yunes, Dark matter or regular matter in neutron stars? how to tell the difference from the coalescence of compact objects, *Phys. Rev. D* **107**, 115028 (2023).
 - [90] M. Vikiaris, V. Petousis, M. Veselsk  y, and C. C. Moustakidis, Neutron star with dark matter admixture: A candidate for bridging the mass gap, *International Journal of Modern Physics D* **34**, 10.1142/s0218271825500646 (2025).
 - [91] A. Maselli, P. Pnigouras, N. G. Nielsen, C. Kouvaris, and K. D. Kokkotas, Dark stars: gravitational and electromagnetic observables, *Phys. Rev. D* **96**, 023005 (2017), arXiv:1704.07286 [astro-ph.HE].